

Vascular phyllotaxis transition and an evolutionary mechanism of phyllotaxis

Takuya Okabe

Faculty of Engineering, Shizuoka University, 3-5-1 Johoku, Hamamatsu 432-8561, Japan

Abstract

Leaves of vascular plants are arranged regularly around stems, a phenomenon known as phyllotaxis. A constant angle between two successive leaves is called divergence angle. On the one side, the divergence angle α_0 of an initial pattern of leaf primordia at a shoot apex is most commonly an irrational number of about 137.5 degrees, called limit divergence. On the other side, the divergence α of a final pattern of leaf traces in the vascular system of a mature stem is expressed in terms of a sequence of rational numbers, $\frac{1}{2}$, $\frac{1}{3}$, $\frac{2}{5}$, $\frac{3}{8}$, $\frac{5}{13}$, $\frac{8}{21}$, called phyllotactic fractions. The mathematical relationship between the initial divergence α_0 , the final divergence α , and the number of internodes traversed by the leaf traces n_c is investigated by means of a theoretical model of vascular phyllotaxis. It is shown that continuous changes of the trace length n_c induce transitions between the fractional orders in the vascular structure. The vascular phyllotaxis transition suggests an evolutionary mechanism for the phenomenon of phyllotaxis. To provide supporting evidence for the model and mechanism, available experimental results for fossil remains of *Lepidodendron* and the vascular structure of *Linum* and *Populus* are analyzed with the model.

Keywords: phyllotaxy; Fibonacci numbers; golden ratio; natural selection; *Linum usitatissimum*; *Populus deltoides*

Email address: `ttokabe@ipc.shizuoka.ac.jp` (Takuya Okabe)

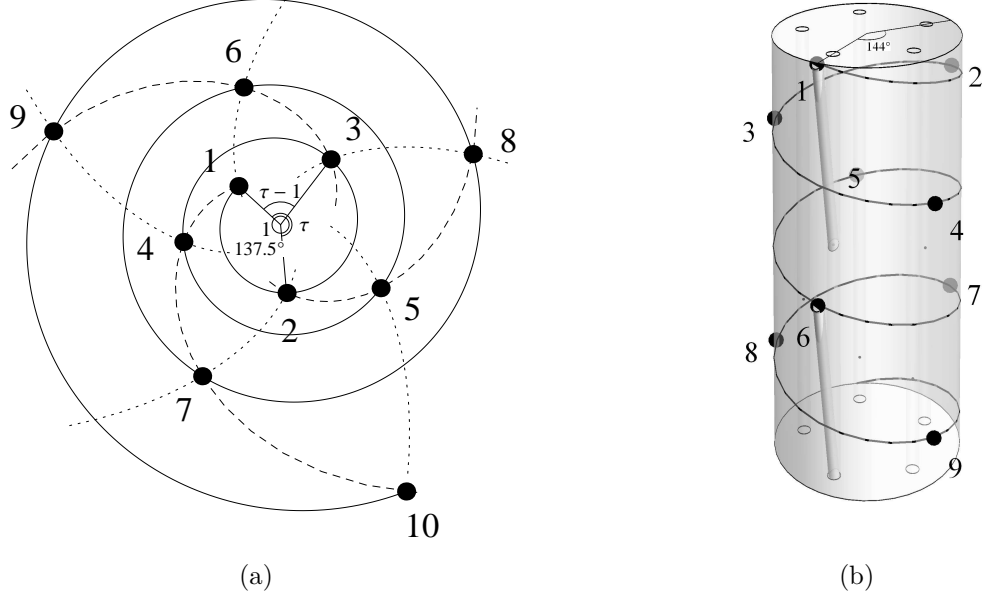


Figure 1: (a) A typical pattern of leaf primordia (points) on a shoot apex with the initial divergence of $\alpha_0 = 1/(1+\tau)$, or $360\alpha_0 \simeq 137.5$ in degrees. The irrational number $\tau \simeq 1.618$ is the golden ratio defined by the proportion equation $1 : \tau = \tau - 1 : 1$. The primordia are numbered in the reverse order of production. A solid spiral connecting all the primordia in the numerical order is the genetic spiral. Three dashed spirals (clockwise inward) and five dotted spirals (counterclockwise inward) are 3 and 5 parastichies, respectively. This pattern has a parastichy pair (3, 5). (b) A typical pattern of leaves on a mature stem characterized with a divergence fraction of $\alpha = \frac{2}{5}$ ($360\alpha = 144^\circ$). Oblique strands diverging to leaves 1 and 6 are leaf traces. A solid spiral surrounding the stem is the genetic spiral.

1. Introduction

1.1. Review, background, and motivation

Astonishing regularity manifested in plant architecture has fascinated various fields of scientists for centuries. The regular arrangement of leaves, flowers and floral organs of higher plants is called phyllotaxis. A constant angle of rotation between two successive organs is called divergence angle, on which two apparently irreconcilable concepts have been in general use since the inception of quantitative investigations on phyllotaxis.

Braun (1831, 1835) and Schimper (1835) noticed that divergence angle is various but not arbitrary. It is a fraction, or a *rational number*, a number that can be expressed as the quotient $\frac{n}{m}$ of two integers n and m . The

most widespread is the helical phyllotaxis, also called spiral or alternate phyllotaxis, in which stems bear a leaf per node. In the helical phyllotaxis, the numerator n and denominator m of the fraction normally are two alternate terms of a Fibonacci sequence, 1, 2, 3, 5, 8, 13, 21, 34, 55, 89, \dots . It is generated by the Fibonacci recurrence relation that each number after the first two terms is the sum of the previous two numbers. The phyllotactic fractions $\frac{1}{2}, \frac{1}{3}, \frac{2}{5}, \frac{3}{8}, \frac{5}{13}, \frac{8}{21}, \frac{13}{34}, \dots$ comprise what is called the main sequence of phyllotaxis. A $\frac{2}{5}$ phyllotaxis is schematically shown in Fig. 1(b). In multijugate, verticillate or whorled phyllotaxis, where more than two leaves are borne at each node, the divergence angle is divided by the number of leaves in a whorl. In general, a plant stem is partitioned into nodes and internodes. A node is a point at which a leaf or leaves are attached, and an internode is a section of the stem between two successive nodes. In the fractional phyllotaxis, there are leaves aligned vertically above each other along a stem, as represented by leaves 1 and 6 in Fig. 1(b). A straight line connecting the superposed leaves is called an orthostichy. In the helical phyllotaxis, the denominator of the phyllotactic fraction is equal to the number of orthostichies. It is also the number of internodes between two adjacent leaves on an orthostichy. Thus, the $\frac{2}{5}$ phyllotaxis in Fig. 1(b) has five orthostichies, 1-6, 2-7, 3-8, 4-9 and 5-10, and five internodes separate leaves on each orthostichy. An imaginary spiral connecting all the leaves in the order of production is called the genetic, fundamental, generative, or ontogenetic spiral. The numerator of the fraction refers to the number of turns of the genetic spiral between the two adjacent leaves on an orthostichy. In Fig. 1(b), a solid spiral is the genetic spiral. From the leaf 6 to 1, the genetic spiral winds around the stem twice, the number two being the numerator of $\frac{2}{5}$. As remarked below, the phyllotactic fraction does not lose its significance even though vertical alignment is actually not exact but approximate.

In contrast, Bravais and Bravais (1837) suggested that divergence angle is uniquely and invariably given by an *irrational number*, that is, a number which cannot be expressed as a fraction. The most typical angle of $360/(1+\tau)$ degrees is called the golden angle, where the irrational number τ , called the golden ratio, golden mean, golden section, or extreme and mean ratio, is defined by the proportional relation $1 : \tau = \tau - 1 : 1$. As the positive solution of the quadratic equation $\tau(\tau - 1) = 1$, it is given by

$$\tau = \frac{\sqrt{5} + 1}{2} \simeq 1.61803399 \dots \quad (1)$$

The defining equation is transformed to $\tau^{-1} = 1/(1 + \tau^{-1})$. Recursive substitution of τ^{-1} in the left-hand side to the right-hand side gives an infinite continued fraction representation,

$$\tau^{-1} = \frac{1}{1 + \frac{1}{1 + \frac{1}{1 + \ddots}}}, \quad \tau = 1 + \tau^{-1}.$$

The golden angle $360/(1 + \tau) = 360/\tau^2$ is approximately 137.50776 degrees. By definition, the golden angle is the smaller angle created by sectioning the circumference of a circle (360 degrees) according to the golden ratio $1 : \tau$, the golden section. A phyllotactic pattern with divergence equal to the golden angle is shown in Fig. 1(a). The ratio of the angle subtended by 1 and 2 to the angle between 1 and 3 is τ , or $\angle 1O2 : \angle 1O3 = 1 : \tau - 1 = \tau : 1$, where O is the origin. Similarly, $\angle 1O4 : \angle 2O4 = \angle 1O9 : \angle 4O9 = 1 : \tau$, and so on. Thus, phyllotactic patterns with constant divergence equal to the golden angle have harmonious proportions. Patterns with an irrational divergence angle have no orthostichy in a strict sense, as no two leaves align vertically or radially. Instead, therefore, attention is directed to secondary spirals connecting positionally nearby leaves, called parastichies. Like an orthostichy, a parastichy is characterized by a difference in number of leaves on it. In Fig. 1(a), the genetic spiral, three parastichies and five parastichies are drawn with a solid curve, dashed curves and dotted curves, respectively. Each of three parastichies 1-4-7-10, 2-5-8 and 3-6-9, is called a 3-parastichy. Hence there are three 3-parastichies and five 5-parastichies in Fig. 1(a), and the pattern in Fig. 1(a) is said to have a parastichy pair of (3, 5), which is also denoted as (3 + 5) or 3 : 5. As a remarkable fact, parastichy numbers are almost always given by Fibonacci numbers. This is a mathematical consequence of the fact that divergence angle is almost always the special irrational number, the golden angle. The golden angle is also called the Fibonacci angle, for it is the limit angle of divergence for the phyllotactic fractions belonging to the main sequence;

$$\begin{aligned} 360 \times \frac{2}{5} &= 144, \\ 360 \times \frac{3}{8} &= 135, \\ 360 \times \frac{5}{13} &\simeq 138.46, \\ 360 \times \frac{8}{21} &\simeq 137.14. \end{aligned}$$

The rational angles beyond $\frac{5}{13}$ are practically indistinguishable from the ‘ideal’ irrational angle of 137.507764... degrees. Therefore, it is argued that

what appear to be different rational angles are nothing but a single irrational angle disturbed by inevitable random errors.

The seemingly conflicting views on the divergence angle, whether rational numbers or an irrational number, are a source of inspiration and confusion. In effect, they are not only compatible but both indispensable. On the one hand, the irrational number applies to the divergence angle of phyllotactic patterns of undifferentiated tissues at shoot tips or apical meristems (Church (1904); Hirmer (1922, 1931)). Let us call it the initial divergence angle. It is commonly referred to as the ideal or limit divergence angle for the reason mentioned above. On the other hand, the rational (fractional) divergence applies to phyllotaxis of leaves, or primary vascular architecture on a mature stem (Lestiboudois (1848); Nägeli (1858)). In the literature, the majority of studies discuss the former, i.e., the process of organ initiation, positioning of the leaf primordia from which leaves will develop, and transitions of patterns at the shoot apical meristem. In recent years, substantial progress has been made in understanding plant hormonal factors that influence or control the formation of leaf primordia and their arrangement on the apical meristem (Reinhardt (2005); Kuhlemeier (2007)). In striking contrast, the fractional phyllotaxis of the mature stem have received less scholarly attention, unfortunately. This is not because the latter is less important than the former. As a matter of fact, experimental findings on the close relationship between phyllotactic fraction and vascular organization have been accumulated without being theorized from a general perspective (Sterling (1945); Girolami (1953); Jensen (1968); Namboodiri and Beck (1968); Larson (1977); Beck et al. (1982); Kirchoff (1984)).

Since the influential text by Hofmeister (1868), research into causal or dynamical mechanisms of primordia initiation has been the central pillar in the study of phyllotaxis. The empirical observation that new leaf primordia arise in the largest space between the older primordia is called Hofmeister's rule. What was originally a rule of thumb of botanists has been refined and developed into causal or dynamical models. Airy (1873) speculated on a causal mechanism in terms of geometrical objects in mechanical action. Schwendener (1878) put a similar idea on a more solid mathematical basis by regarding leaves on a stem as solid disks contiguously covering a cylinder surface of infinite length (Fig. 2). In Schwendener's model, contiguous circles of a constant radius are arranged in a periodic pattern characterized with a given set of contact parastichy numbers. Then it is a purely geometrical problem to derive various mathematical relations for the divergence angle,

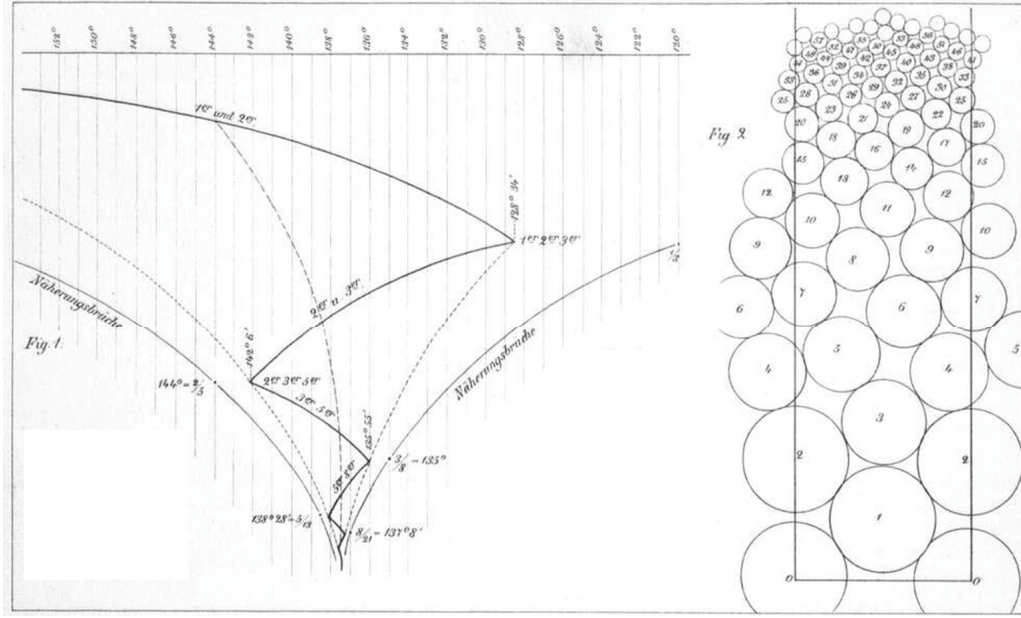


Figure 2: Schwendener's causal model. Right: Contiguous circles with decreasing radius are stacked on an unrolled surface of a stem cylinder. Contact parastichy numbers, or differences in the numbers of the circles in contact, change from (1,1) at the bottom to (5,8) at the top. Left: A mathematical relation between the divergence angle (the horizontal axis) and the radius of the contiguous circles (the vertical axis) is indicated with a solid zigzag curve starting from the top left corner (divergence of 180° , corresponding to the bottom part of the right figure) down to the golden angle 137.5° (the top of the right figure). The zigzagging is due to shifts in the contact parastichy numbers from (1,1) through (1,2), (2,3), (3,5), (5,8), (8,13), (13,21) to (21,34). The top branch for (1,2) extends from 180° to $128^\circ34'$. Adapted from Schwendener (1883).

the radius of the circles, the girth of the cylinder, and the set of parastichy numbers. The radius of the circles is regarded as an independent variable, or a control parameter of the model. By letting the radius change continuously along the stem cylinder, the divergence angle varies concomitantly with the contact parastichy numbers according to the mathematical relations. As a remarkable result, the divergence angle converges toward the golden angle 137.5° by decreasing the radius sufficiently slowly from a large initial value to a small constant value. Before attaining to the golden angle, the model predicts that the divergence angle oscillates with decreasing amplitude (Fig. 2). The decrease in the radius corresponds to decrease in relative size of leaf primordia on the stem or apex. This is a brief summary of Schwendener's causal mechanism for the golden angle. The model is referred to as a mechanical or causal model of phyllotaxis.

Related causal models were discussed in depth by Delpino (1883) and van Iterson (1907). In recent decades, models of Schwendener and van Iterson have been elaborated on and developed further mathematically (Adler (1974); Rothen and Koch (1989); Levitov (1991); Kunz (2001); Atela et al. (2002)) or numerically (Williams and Brittain (1984); Hellwig et al. (2006)), and even realized dynamically in a physics laboratory experiment (Douady and Couder (1996)). The causal models are founded on the basic assumption of causal determinism that a phyllotactic pattern is a result of causal interaction of pattern units. In particular, the position of an initiated leaf primordium is determined by the position of the older primordia according to (supposedly simple) causal rules. The manner in which the units are arranged depends on the dynamic history of growth, or particularly on the course of changes in size of leaf primordia. Thus, a common key factor of the causal models is a gradual change in size of leaf primordia under mutual repulsion. Accordingly, there is a variety of causal models in which the repulsive interaction is ascribed not to the mechanical contact pressure as supposed by Airy and Schwendener, but to a chemical diffusion process (Schoute (1913); Thornley (1975); Mitchison (1977); Veen and Lindenmayer (1977); Young (1978); Marzec and Kappraff (1983); Schwabe and Clewer (1984); Chapman and Perry (1987); Roberts (1987); Steeves and Sussex (1989); Yotsumoto (1993); Koch and Meinhardt (1994); Meinhardt et al. (1998)). There are another causal models based on physical (Hofmeister (1868); Green et al. (1996); Newell et al. (2008)) and chemical (Cummings and Strickland (1998)) instabilities. Recently, more intricate models based on molecular-genetic experiments have been discussed (Smith et al. (2006a,b); Jönsson et al. (2006); Shipman et al. (2011)), while

geometrical models have been used to interpret patterns of real systems (Malygin (2006); Hotton et al. (2006); Zagórska-Marek and Szpak (2008)). All these causal models are based on the assumption that *divergence angle is intrinsically variable and determined causally*.

In the recent literature, we have had few opportunities of finding phyllotactic fractions in use. Most theoretical and experimental works attach importance to parastichy numbers instead, and the phyllotactic fraction is not mentioned or regarded merely as an approximation even if mentioned (Williams (1974); Steeves and Sussex (1989); Lyndon (1990); Jean (1994)). The fractional phyllotaxis is the original problem. There are some reasons for this trend. First, early researchers did not appreciate the structural significance of the phyllotactic fraction (Hofmeister (1868); de Candolle (1881); Church (1920); Hirmer (1922); Richards (1951); Snow (1955)). Second, the studies of vascular structure organization are comparatively so few in number that they are overshadowed by intensive research interests directed towards the shoot apical meristems. Third, Schwendener's causal model and its descendants are at variance with the fractional divergence. According to the model, the divergence angle varies depending on size of leaves, the vertical coordinate of Fig. 2. Schwendener (1883) guessed that a fractional pattern would be made secondarily as a result of mechanical straightening of parastichous bundles connecting initiated leaves. Teitz (1888) confirmed indeed that the fractional phyllotaxis is accomplished by secondary torsion occurring in the vascular system during growth of the stem. When there is little or no secondary distortion for lack of subsequent growth or internodal elongation, the original pattern at the apex may grow to a similar pattern of mature organs. This holds true for the most eye-catching patterns of closely packed reproductive organs, which, therefore, are often compared favorably with numerically simulated outputs of causal models. Even then, the basic concept of the phyllotactic fraction may remain significant internally in vascular connections (Watson and Casper (1984)). In fact, a stem with short internodes takes a high-order fraction, which can be indistinguishable from the limit divergence of the undistorted stem. Thus, the phyllotactic fraction may not be judged by the external appearance alone.

In vascular plants, each leaf is connected to the main stem vascular system through a strand of fluid-carrying vascular tissue called a leaf trace. A leaf may have several to many leaf traces. Leaf traces diverge from the stem vascular system some distance below or very near the nodes at which they enter the leaves (Lestiboudois (1848); Nägeli (1858); Beck (2010)). At

the level of the shoot apex, leaf traces form parastichous strands winding obliquely round the stem axis. As the stem elongates, the leaf traces align up along the stem to make orthostichous bundles by forcing the whole stem to twist slightly from the original pattern (Fig. 1(b)), thereby a phyllotactic pattern characterized by a phyllotactic fraction is established. In the final pattern, there is a definite relationship between the denominator of the phyllotactic fraction and the number of vascular orthostichies (Kirchoff (1984)). The term orthostichy might be misleading, because the straightened bundles still may maintain their tilted course. The fraction neatly represents geometrical arrangement of leaf traces, and the fractional order need not mean that leaves are positioned exactly vertically. Developmental sequences in differentiation and vascularization of leaf primordia are numerically correlated with the phyllotactic fraction of the shoot (Priestley and Scott (1936); Girolami (1953); Esau (1965)). Seemingly irregular rhythmical variations in various lengths of the external structure of a mature plant may be understood as a consequence of a hidden phyllotactic order in the vascular system (Unruh (1950); Kumazawa and Kumazawa (1971)). There is evidence for restricted pathways of translocation of photosynthetic assimilates related to phyllotaxis (Watson and Casper (1984)). The patterns of translocation are sectorial, or the phyllotactic fraction has biological significance. The observation most pertinent to the present work is the significant correlation existing between the phyllotactic fraction and the number of internodes traversed by leaf traces: The higher phyllotactic fractions are associated with the longer leaf traces (Girolami (1953); Esau (1965)). While leaf traces of plants with helical phyllotaxis typically traverse more than one internode, in distichous phyllotaxis, a $\frac{1}{2}$ phyllotaxis of two-ranked leaf arrangement, and in verticillate phyllotaxis, leaf traces are approximately one internode or less (Beck et al. (1982)). Accordingly, low-order systems of a $\frac{1}{2}$ and $\frac{1}{3}$ phyllotaxis are seen on the stems of plants with long internodes, while plants with short internodes show high-order fractions, as remarked above.

The stem vascular bundles, or axial bundles, and associated leaf traces comprise sympodia, on the nature of which there are two perspectives (Beck (2010)). In one view, the sympodia are of cauline origin, or derived from stem vascular tissue (Beck et al. (1982)). In the other view, they are of foliar origin, or derived from leaf traces (Esau (1965)). There are two different views on the causal relation between initiation of primordia and development of leaf traces or procambial strands, the strands differentiating into vascular bundles of xylem and phloem. In one view, the initiation of leaf

primordia brings about the differentiation of the leaf traces. Hence the initiation of the leaf traces occurs basipetally, or in the direction from the leaf primordia toward the vascular system of the stem. In the opposing view, phyllotaxis of leaf primordia is dictated by the vascular organization that has been established before the leaf primordia are initiated (Larson (1977, 1983)). The latter is consistent with the observation that an incipient leaf trace develops acropetally, or in the direction toward the leaf primordium it serves (Esau (1965); Nelson and Dengler (1997)). Priestley and Scott (1933) was criticized by Snow and Snow (1934). They both do not cast doubt on Hofmeister's rule, that is, they share the causal view that phyllotaxis is a natural consequence of growth and development of an individual plant. They differ in what they regard as a basic unit of phyllotaxis. The former adopts growth units including leaf traces, while the latter places primary emphasis on leaf primordia at the apex. Accordingly, the former and the latter attach little importance to the irrational and rational divergence, respectively. Thus, the causal view has been the paradigm of phyllotaxis.

On the whole, causal models are successful in deriving indefinitely continuing stable systems, resembling actual phyllotactic patterns. From a computational point of view, they are particularly appealing in that they provide us with programmable protocols leading to the golden angle. Irrespective of detailed mechanisms, however, realistic phyllotactic patterns are derived based on the following observational facts (Vogel (1979); Rivier et al. (1984); Prusinkiewicz and Lindenmayer (1991)): (i) Divergence angle is constant. (ii) The constant is the golden angle. For the sake of argument, the former is often taken so broadly that the constant may take any value. On this premise, phyllotaxis is rendered to a geometrical playground of mathematics. There are mathematical arguments for (ii) based on the generalized hypothesis (i) (de Candolle (1881); Coxeter (1972); Leigh (1972); Ridley (1982); Marzec and Kappraff (1983)). It is often stated in this regard that the golden angle is a special angle at which optimal packing is achieved. As a matter of fact, this is not true literally, for it is only under the constraint (i) that the golden angle may be said optimal and there is no *a priori* reason for the constancy. For living organisms, the property (i) is far from obvious and no less astounding than (ii), especially because the angular regularity may persist in spite of temporal irregularity. A time interval between the formation of successive leaves is called a plastochron, which is used as a morphological or developmental time scale. Plants grown in different environmental conditions may be compared in plastochron units but not in physical time units. The

fact that unit of time is a plastochron and duration of a plastochron is not constant in physical time poses a problem for realistic causal models based on physical time.

Phyllotactic patterns at a shoot apex are more regular than those on a mature stem, because internodes tend to be elongated less regularly on the mature stem. As a matter of fact, the exact level in the stem at which a bifurcation or recombination of vascular bundles takes place is not an important morphological constant (Dormer (1972)). Accordingly, trace lengths may vary arbitrarily along the stem. For this reason, it is often argued that one should devote oneself exclusively to the study of the growing apex (Church (1904); Snow (1955)). Nonetheless, further mathematical relations for the spiral patterns at the apex can be derived by assuming a stronger mathematical constraint of exponential growth, according to which the leaf primordia are arranged on logarithmic spirals in a centric representation (Fig. 1(a)) (Church (1904); Richards (1951); Thomas (1975); Jean (1994)). In the exponential growth, the ratio of the distances from the center of the apex to two successively numbered primordia is a constant, called the plastochron ratio. For a fixed value of divergence angle, Richards (1951) has advocated the use of a phyllotaxis index defined in terms of the plastochron ratio (cf. (A.1)). The index is used to designate two sets of parastichies intersecting orthogonally. For instance, for Fig. 1(a), the plastochron ratio is 1.2, the phyllotaxis index is 3, and (3, 5) parastichies cross at right angles. A fractional value of the index, such as 2.7, means that no two parastichies are orthogonal. In this geometrical model, a shift in parastichy numbers, e.g. from (3, 5) to (5, 8), a phenomena called rising phyllotaxis, is related to a variation of the plastochron ratio, or the exponential growth rate. The model has been generalized to allow for other constant divergence angles than the golden angle (Richards (1951); Thomas (1975); Jean (1994)). In contrast to these geometrical models based on *constant* divergence angle, there exist geometrical causal models in line with Schwendener's model, which aim at deriving the limit divergence angle by assuming *variable* divergence angles depending on plastochron, the plastochron ratio, and their own rules (van Iterson (1907); Williams (1974); Erickson (1983); Williams and Brittain (1984)). For a vegetative shoot, a plastochron index is defined in terms of length of leaves, and a leaf on a shoot is labeled with a leaf plastochron index (Erickson and Michelini (1957)). A developmental index of this kind is indispensable for the systematic study of plant development (Meicenheimer (2006)). The exponential growth is a practically useful approximation in

dealing with young organs and early stages of development, although it is neither essential nor peculiar to phyllotaxis.

Despite the apparent success of causal models, neither their intrinsic mechanisms nor predictions have yet been subjected to experimental tests specifically. To name several problems on a descriptive level, existing causal models that explain all types of observed patterns cannot help predicting also a multiplicity of unreal or too rare patterns. Even when they are capable of deriving normal patterns, they are not free from instabilities apparently irrelevant to living organs. Causal models in general are confronted with a subtle trade-off. Normal phyllotactic patterns must be stable enough to account for the current prevalence in nature, while they cannot be quite stable in order to allow for many other exceptional ideal angles just to such a degree that they are actually existent. In short, rare patterns should be neither too common nor too rare. It is not clear how and why this subtle balance between stability and instability is maintained universally, since fine control of relative size of phyllotactic units depends not only on species but individual plants or even on parts of the individual plant. We get puzzled all the more by the observations of more frequent occurrence of rare patterns among fossil plants.

Causal models, whether physical or chemical, provide dynamical schemes of self-adjusting the system under the influence of the older leaf primordia. On the premise that divergence angles between successive leaves are freely variable by nature, they aim to derive a special angle, normally the golden angle, toward which the variable divergence angles tend ultimately. They do not assume any special constant divergence *a priori*. For the very reasons, they are likely to be beset with a fundamental difficulty in protecting the system against disturbance. In this regard, Hofmeister's empirical rule is often overestimated. Observed patterns satisfy Hofmeister's rule, but Hofmeister's rule is not sufficient for observed patterns. Hofmeister's rule does not imply the *periodic* appearance of new primordia (Kirchoff (2003)), nor does it ensure precise regulation of the divergence of 137.5° (cf. Fig. 12(a)). It is not difficult to draw an unreal pattern according to Hofmeister's rule. The remarkable empirical fact is rather that divergence angle during steady growth seems always regulated stably to one of special angles closely related to the golden ratio. In fact, if a causal rule is to be strictly applied throughout, fluctuations in size of the domain of influence of a leaf primordium should inevitably leave behind everlasting irregularities propagated in the developing pattern (Snow and Snow (1962)). Mathematically, the instability is a general

consequence of the fact that the number of possible phyllotactic configurations proliferates as relative size of phyllotactic units decreases. According to causal interpretations, higher phyllotaxis becomes more vulnerable. The difficulty may not be obvious if one were interested only in low-order patterns like a (2, 3) and (3, 5) phyllotaxis, but it should become conspicuous when dealing with a higher order pattern which requires higher precision maintenance. Besides this stability problem for high-order patterns, causal models have another difficulty for low-order patterns (Sec. 3).

There are apparent geometric correlations between parastichy numbers and relative size of primordia on the apex (Church (1904); Richards (1951); Kirchoff (2003)) and between leaf arcs and the plastochron ratio (Rutishauser (1998)). Causal models implement them as causal relationships with the intention of proving that a phyllotactic pattern, especially the divergence angle of 137.5° , is a necessary consequence of changes in the causal agent, relative size of leaf primordia. According to this interpretation, divergence angles and contact parastichies must depend not only on the shape of primordia but on the geometry of the surface on which they are located. The dependence has been investigated by van Iterson (1907) on the assumption that all the primordia keep a common shape while they are allowed to change their sizes. So far, however, no direct evidence has been provided to support the presumed causal relationship. As a matter of fact, there are very few studies in which sufficiently detailed data are obtained to make a close comparison with the models possible or useful (Erickson (1983)). In particular, the prediction of causal models that rising phyllotaxis, or change in parastichy numbers, should accompany wide variations and abrupt turns of divergence angle, as indicated in Fig. 2, has not been supported unequivocally. On the contrary, the success of Richards' model indicates the exponential growth with *constant* divergence angle irrespective of whether parastichy numbers rise or fall. Church (1904) refuted Schwendener's model by counterexamples showing normal spiral patterns of circular primordia whose positions are widely separated. In comparing treated plants, Maksymowych and Erickson (1977) found no significant change in divergence angle in a correlation diagram for the plastochron ratio and divergence angle. Statistical analysis of Fujita (1939) has revealed that divergence angles do not depend so much on parastichy numbers as expected from causal models (Jean (1986)). There is clear evidence against the basic assumption that the primordia size is the causal factor of divergence angle. A plant appears to accomplish geometrical correlations in a phyllotactic pattern by adapting the size and shape of

leafy organs as if it knows the end pattern at which it aims. Snow and Snow (1962) observe that the secondary extension of a leaf base adjusts itself so that divergence angle is little affected in spite of artificial disturbances. This observation, despite the authors' claim, undermines their space-filling mechanism that the leaf base extension regulates the phyllotactic pattern. To the contrary, apparent causal changes in the position, size and shape of leaves or scales in chemical or physical contact may be just incidental phenomena (Church (1904); Richards (1948); Marc and Hackett (1991)). No doubt there are cases in which physical or chemical contact pressure may induce secondary displacement of compactly packed lateral organs.

Natural selection plays no role in causal interpretations of phyllotaxis. If one supposes to the contrary that natural selection holds the key to understanding the golden angle at the shoot apex, then one should investigate a special effect of the special angle, instead of its cause. In other words, one should look for the distal or ultimate cause of the special angle, instead of the proximity cause. This sort of theory intends to explain special traits not in terms of immediate physiological factors, but in terms of evolutionary forces acting on them. It aims at a full understanding of the phenomena at a phenomenological level, independently of whatever physiological mechanisms may be involved. There is a long history of investigations into selective advantage of the observed divergences based on the external structure. It goes as follows: common phyllotactic patterns distribute leaves as evenly as possible and maximize exposure of leaves to enhance the capacity to intercept sunlight (Wright (1873)). Such an argument is unpromising because leaves are aligned in vertical ranks. Indeed, changes in leaf shape and stem length can compensate for the negative effects of leaf overlap (Niklas (1988, 1998)). For this obvious reason, it is often argued to the contrary in favor of the 'most irrational' divergence angle; no two leaves lie precisely under one another when divergence angle is equal to the golden angle (de Candolle (1881); Wiesner (1875, 1907); Coxeter (1972); Leigh (1972); Takenaka (1994); Percy and Yang (1998); Valladares and Brites (2004); King et al. (2004); Bryntsev (2004)). There is also a long history of criticism of this view (Thompson (1917)). In the first place, the golden angle is not a general rule for mature shoots, and the light-capture mechanism deepens the riddle of the common occurrence of a $\frac{2}{5}$ phyllotaxis. In general, existing theories tend to argue for the uses of irrational angles without regard to the uses of rational angles or vice versa.

1.2. Aim and scope of this paper

Let us direct attention to the internal structure, the vascular system. Mathematical interrelationship between the initial (apical) and the mature (vascular) phyllotactic pattern seems to have not been discussed experimentally nor theoretically. This paper develops a theory of vascular phyllotaxis to fill in the gap between the two distinct but intimately related phenomena. A physical model has been described mathematically in the previous paper (Okabe (2011)). However, the model was abstract and its relevance to real phenomena was not clearly elucidated. The aim of this paper is to develop the model to show its experimental validity and relevance. This is relevant to a fundamental problem of phyllotaxis: *Is phyllotaxis determined causally or genetically?* In contrast to numerous models holding the causal view, the present model is based on the genetic perspective that special numbers in phyllotaxis are primarily of genetic origin, so that it is assumed that constant primordial divergence angle during steady growth is genetically determined. According to the model, the effect of constant divergence angle is investigated, and what value of the constant is advantageous is settled. This work is not concerned about transient fluctuations of divergence angle during ontogeny. Therefore, the model is compatible with any physical or chemical causal models for the positioning of leaf initiation at the shoot apex, although the limit divergence angle at the apex is interpreted totally differently. The special angle is not an inevitable consequence of ontogenetic dynamics, whether physical or chemical. It is regarded as a heritable trait of a plant. It is supposed that once there was a wide variation in the traits of individuals, or there have formerly been wide variations of divergence angles. The special limit divergences found in nature have survived natural selection. This conforms with the traditional view that biological features that are under tight genetic control and that have very narrow ranges of variation are believed to be adaptive (Niklas (1997)). Although the author believes that the premise of the model, divergence angle as a trait of a plant, is not only plausible but supported by circumstantial evidence, it has not been unanimously accepted at present. It may be verified or refuted experimentally in the future.

For the efficient transport of materials throughout an indefinite number of leaves attached to a stem of a finite cross section, the leaves should be aligned along a finite number of ‘orthostichious’ bundles. At this point, a whole number enters the theory. There are modes of orthostichous order depending on the initial arrangement and length of leaf traces. The number of

vascular orthostichies may be increased or decreased, but not arbitrarily. By regarding a leaf primordium and the leaf trace(s) associated with it as the fundamental unit of phyllotactic patterns, a mathematical correspondence is derived between the divergence angle of the initial phyllotactic pattern, $360\alpha_0$ degrees, and the phyllotactic fraction α of a mature pattern, where the number of internodes traversed by the leaf traces, n_c , plays a pivotal role. As a general rule, it has been known that phyllotactic fraction of a vascular plant may vary sequentially during growth (Braun (1835); Skutch (1927); Allard (1942); Puławska (1965); Larson (1977)). By means of the mathematical relation between α_0 (an irrational number) and α (rational numbers), it is shown that changes in n_c cause the phyllotactic transitions in α . As a natural consequence, an evolutionary mechanism for the phenomenon of phyllotaxis is suggested. Supporting evidence for the model and the evolutionary mechanism is presented by analyzing experimental results.

In Sec. 2, a model and results used in the following sections are presented by means of figures and tables without using mathematics. Tables 1~18 have not been presented before.

In Sec. 3, observed precision of the initial divergence α_0 is explained by means of a correlation predicted between the range of α_0 and the highest-order fraction α . In short, divergence angle α_0 of a system with a high phyllotactic fraction α should be accurately controlled in order to avoid unnecessary changes in vascular structure.

In Sec. 4, phyllotaxis of *Lepidodendron* by Dickson (1871) is analyzed. Diversity of phyllotaxis is discussed as a result of ineffective selective pressures.

In Sec. 5, the vascular structure of *Linum usitatissimum* by Girolami (1953) is investigated. Various relations between phyllotactic fraction and parastichy numbers, the phyllotactic fraction α and the length per internode of leaf traces n_c , and directions of parastichies and the genetic spiral are pointed out.

In Sec. 6, the phyllotactic transition of *Populus deltoides* by Larson (1977) is analyzed. It is shown that a continuous change in length of leaf traces causes the discontinuous effect of the phyllotactic transition in the vascular structure.

In the appendix, a relation between the trace length n_c and the plastochron ratio a is discussed to indicate that the former serves as a useful developmental index for the mature stem as the latter is used for the apex.

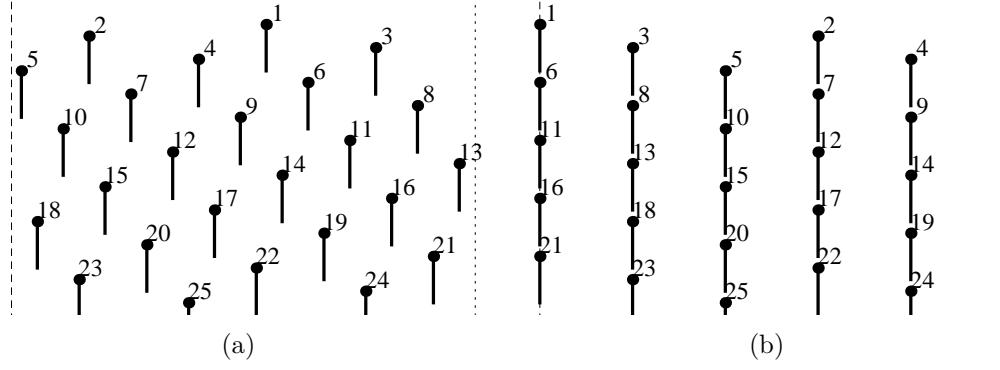


Figure 3: Phyllotactic patterns of leaf traces with a length of $n_c = 4$ before and after secondary torsion are arranged side by side. A dotted and dashed line of each figure represent a vertical cut of a cylinder surface unrolled. (a) A pattern with initial divergence of $360\alpha_0 \simeq 137.5^\circ$ ($\alpha_0 = 1/(1+\tau) \simeq 0.382$). (b) The final pattern of a fractional divergence $\alpha = \frac{2}{5}$ resulting from (a). Leaf traces in the upper part move rightward while the pattern (a) becomes (b), thereby five 5-parastichies in (a), such as 1-6-11-16-21, align themselves to make five orthostichies in (b).

2. Model

A regular helical pattern of leaf traces is schematically plotted as a lattice of line segments on an unrolled surface of a cylinder. The divergence angle of the initial pattern is denoted as $360\alpha_0$ in degrees, which is assumed to be less than 180 degrees, i.e., $0 \leq \alpha_0 \leq \frac{1}{2}$ without loss of generality. Fig. 3(a) presents a typical pattern for $360\alpha_0 \simeq 137.5^\circ$ ($\alpha_0 \simeq 0.382$). The length of leaf traces measured in internodes is denoted as n_c in accordance with the previous notation (Okabe (2011)). As in Fig. 1(b), $n_c = 4$ in Fig. 3. The trace length n_c need not be an integer; n_c is the average number of leaf traces cut by a transverse section (Fig. 4). As the number in a section is an integer, this method gives a good estimate of n_c particularly for $n_c \gg 1$. The model comprises two parameters α_0 and n_c . For the sake of argument, patterns with constant values of them are considered below. Effects of their fluctuations may be discussed based on results to be obtained.

The leaf traces repel with each other laterally to arrange themselves in an orthostichous pattern. The mutual interaction is likely to be regulated by the plant hormone auxin (Beck (2010)). Fig. 3(b) is the final pattern resulting from Fig. 3(a). Divergence of the final pattern is expressed in terms of the phyllotactic fraction α . The pattern of Fig. 3(b) is characterized with

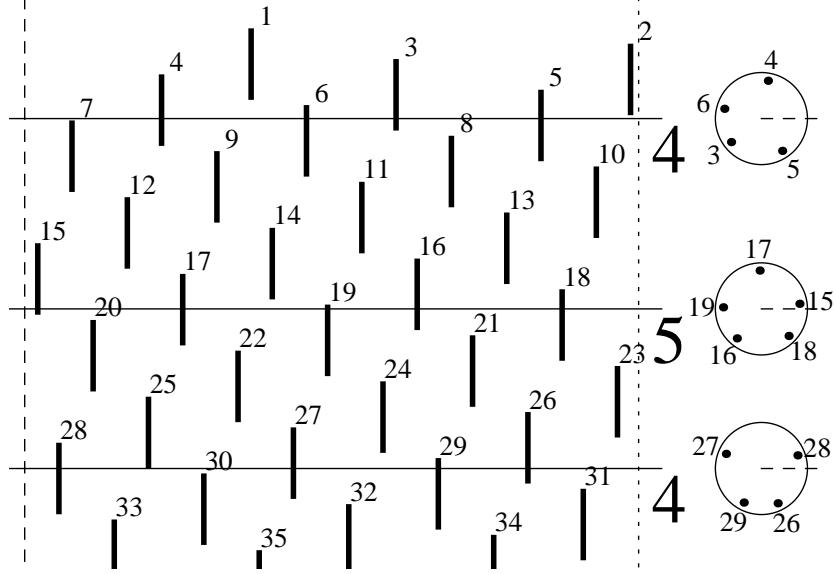


Figure 4: For three transverse sections of a pattern of leaf traces with a length of $n_c = 4.3$, the number of the traces in each section is indicated on the right-hand side below the cut line. The number averaged over sections should approach n_c .

$\alpha = \frac{2}{5}$. In Fig. 3(a), there are five parastichies of 1-6-11-16-21, 2-7-12-17-22, 3-8-13-18-23, 4-9-14-19-24 and 5-10-15-20-25, each of which is called a 5-parastichy. The five 5-parastichies are lined up vertically to make five orthostichies of the $\frac{2}{5}$ phyllotaxis in Fig. 3(b). In the patterns of Fig. 3, the next visible parastichies are 3-parastichies (1-4-7-10-13-16-19-22-25, 2-5-8-11-14-17-20-23 and 3-6-9-12-15-18-21-24) and 2-parastichies (1-3-5-7-9-11-13-15-17-19-21-23-25 and 2-4-6-8-10-12-14-16-18-20-22-24). As these parastichies remain conspicuous in the two patterns, both patterns may be referred to as having a parastichy pair of (2, 3). Thus, for $n_c = 4$, there is one-to-one correspondence between $\alpha_0 \simeq 0.382$ (angle of $360\alpha_0 \simeq 137.5^\circ$) of the initial pattern and $\alpha = \frac{2}{5}$ of the final pattern. In a similar manner, α is obtained for arbitrary values of α_0 and n_c . Indeed, we get $\alpha = \frac{2}{5}$ insofar as $3 \leq n_c < 5$ and $\frac{1}{3} < \alpha_0 < \frac{1}{2}$ (see Okabe (2011) for the mathematical implementation). Below we discuss phyllotactic changes in α that occur when n_c and α_0 are set out of their respective ranges.

For a fixed value of $\alpha_0 \simeq 0.382$, Fig. 5(a) is for $n_c = 7$ in comparison with Fig. 3(a) for $n_c = 4$. As the traces of length longer than five internodes

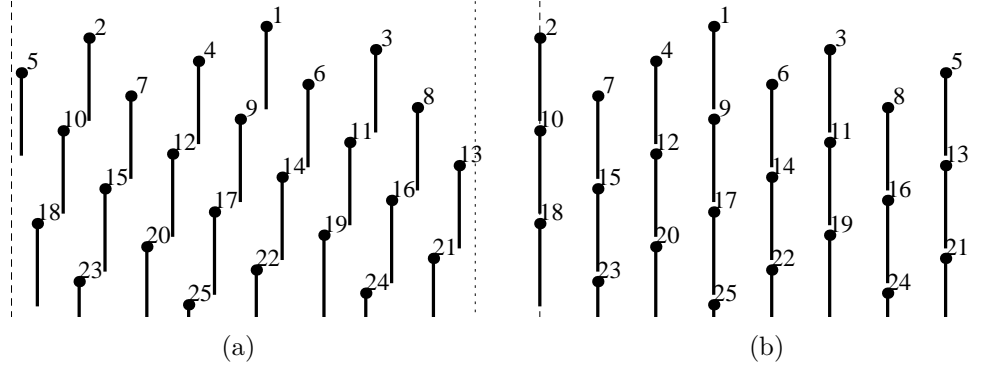


Figure 5: Change in a phyllotactic pattern of leaf traces with a length of $n_c = 7$ (cf. Fig. 3). (a) The initial pattern with $\alpha_0 = 1/(1 + \tau) = 1/(2 + \tau^{-1})$ ($360\alpha_0 \simeq 137.5^\circ$). (b) The final pattern with $\alpha = \frac{3}{8}$.

cannot be aligned in five orthostichies, we obtain $\alpha = \frac{3}{8}$ for Fig. 5(a), while $\alpha = \frac{2}{5}$ in Fig. 3(a). Thus, it is explained that a higher phyllotactic fraction is obtained for a longer length of leaf traces. Phyllotactic transition from $\alpha = \frac{2}{5}$ to $\alpha = \frac{3}{8}$ occurs when n_c increases past a threshold value of $n_c = 5$. Experimental evidence of this transition is presented below in Fig. 17.

For a fixed value of n_c , the phyllotactic fraction α depends on the initial divergence α_0 . For $n_c = 4$, Fig. 6 is for $\alpha_0 \simeq 0.276$ (angle of 99.5°), which is compared with Fig. 3 for $\alpha_0 \simeq 0.382$ (137.5°). The former leads to a final pattern of $\alpha = \frac{2}{7}$ in Fig. 6(b), while the latter gives $\alpha = \frac{2}{5}$ in Fig. 3(b). In fact, there are three fractional patterns conceivable for $n_c = 4$, namely (a) $\alpha = \frac{1}{5}$ for $0 < \alpha_0 < \frac{1}{4}$, (b) $\alpha = \frac{2}{7}$ for $\frac{1}{4} < \alpha_0 < \frac{1}{3}$ and (c) $\alpha = \frac{2}{5}$ for $\frac{1}{3} < \alpha_0 < \frac{1}{2}$.

Every phyllotactic fraction for α has its own ranges of values for α_0 and n_c . The mathematical correspondence is presented succinctly as a tree diagram in Fig. 7. For instance, Fig. 7 gives the conditions $\frac{1}{4} < \alpha_0 < \frac{1}{3}$ and $4 \leq n_c < 7$ for $\alpha = \frac{2}{7}$. For the former inequalities, the boundary fractions $\frac{1}{4}$ and $\frac{1}{3}$ lie below $\frac{2}{7}$ in Fig. 7. The latter condition $4 \leq n_c < 7$ is reasoned from the vertical coordinate $n_c = 4, 5$ and 6 of three $\frac{2}{7}$'s in Fig. 7. The phyllotactic sequence of fractions derived from an arbitrary value of initial divergence α_0 may be traced by climbing up the tree of Fig. 7 along the vertical line at α_0 . For $\alpha_0 \simeq 0.382$ (137.5°), the main sequence $\frac{1}{2}, \frac{1}{3}, \frac{2}{5}, \frac{3}{8}, \frac{5}{13}, \frac{8}{21}, \dots$ is obtained in the increasing order of n_c . The tree diagram extended for all values of n_c includes all conceivable phyllotactic fractions.

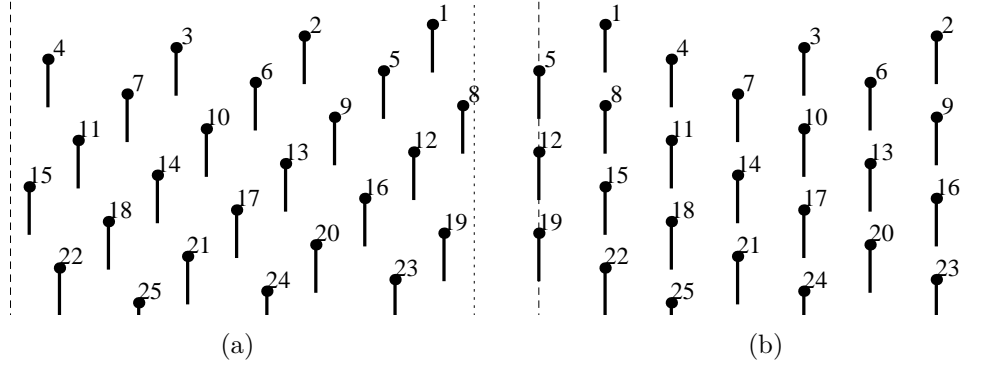
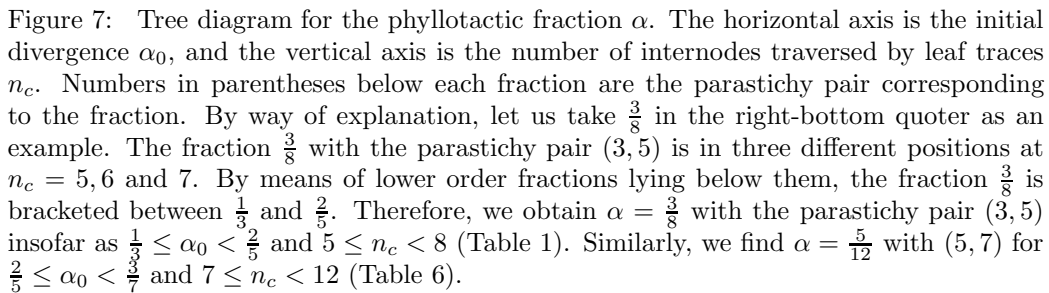


Figure 6: Change in a phyllotactic pattern of leaf traces with a length of $n_c = 4$ (cf. Fig. 3). (a) The initial pattern with $\alpha_0 = 1/(3 + \tau^{-1}) \simeq 0.276$ ($360\alpha_0 \simeq 99.5^\circ$). (b) The final pattern with $\alpha = \frac{2}{7}$.

For the sake of convenience, let us introduce shorthand notation for the irrational numbers found in nature,

$$\begin{aligned}
 [n] &\equiv \frac{1}{n + \tau^{-1}}, \\
 [n, m] &\equiv \frac{1}{n + \frac{1}{m + \tau^{-1}}}, \\
 [n, m, l] &\equiv \frac{1}{n + \frac{1}{m + \frac{1}{l + \tau^{-1}}}}, \tag{2}
 \end{aligned}$$

and so on, where n, m, l are positive integers. With this notation, $\alpha_0 = [2] = 1/(2 + \tau^{-1}) = 1/(1 + \tau)$ gives the main sequence. The last equality holds by the definition of τ in (1). Note that the pattern with $\alpha_0 = [1]$ ($360\alpha_0 = 222.5^\circ$) is nothing but the mirror image of $\alpha_0 = [2]$ (137.5°), because $[1] = 1 - [2]$ or $222.5^\circ = 360^\circ - 137.5^\circ$. For future reference, Tables 1~18 are provided for the initial divergence α_0 given by typical irrational numbers. These are not exhaustive, but they include almost all phyllotactic fractions observed in nature. The main sequence is presented in Table 1. In the second column for $\alpha = \frac{2}{5}$, ‘(2, 3)’ in the second row represents the parastichy pair corresponding to the fraction $\frac{2}{5}$, ‘3 ~’ in the third row abbreviates $3 \leq n_c < 5$, where 5 for the upper limit is taken from the next column, and ‘ $\frac{1}{3} \sim \frac{1}{2}$ ’ in the fourth row



α	$\frac{2}{5}$	$\frac{3}{8}$	$\frac{5}{13}$	$\frac{8}{21}$	$\frac{13}{34}$	$\frac{21}{55}$	$\frac{34}{89}$	$\frac{55}{144}$
	(2,3)	(3,5)	(5,8)	(8,13)	(13,21)	(21,34)	(34,55)	(55,89)
n_c	3 ~	5 ~	8 ~	13 ~	21 ~	34 ~	55 ~	89 ~
α_0	$\frac{1}{3} \sim \frac{1}{2}$	$\frac{1}{3} \sim \frac{2}{5}$	$\frac{3}{8} \sim \frac{2}{5}$	$\frac{3}{8} \sim \frac{5}{13}$	$\frac{8}{21} \sim \frac{5}{13}$	$\frac{8}{21} \sim \frac{13}{34}$	$\frac{21}{55} \sim \frac{13}{34}$	$\frac{21}{55} \sim \frac{34}{89}$

Table 1: Parastichy numbers (in parentheses) and ranges of n_c and α_0 for the phyllotactic fractions α belonging to the main sequence with the limit divergence of $\alpha_0 = [2] = 1/(2 + \tau^{-1}) \simeq 0.3820$ ($360\alpha_0 \simeq 137.5^\circ$). The parastichy pairs are generated from the seed pair (1, 2) for $\alpha = \frac{1}{3}$ (not shown) by a Fibonacci recurrence relation. The golden angle $\alpha_0 = [2]$ and the main sequence are called the Fibonacci angle and the Fibonacci sequence.

α	$\frac{1}{4}$	$\frac{2}{7}$	$\frac{3}{11}$	$\frac{5}{18}$	$\frac{8}{29}$	$\frac{13}{47}$	$\frac{21}{76}$	$\frac{34}{123}$
	(1,3)	(3,4)	(4,7)	(7,11)	(11,18)	(18,29)	(29,47)	(47,76)
n_c	3~	4~	7~	11~	18~	29~	47~	76~
α_0	$0 \sim \frac{1}{3}$	$\frac{1}{4} \sim \frac{1}{3}$	$\frac{1}{4} \sim \frac{2}{7}$	$\frac{3}{11} \sim \frac{2}{7}$	$\frac{3}{11} \sim \frac{5}{18}$	$\frac{8}{29} \sim \frac{5}{18}$	$\frac{8}{29} \sim \frac{13}{47}$	$\frac{21}{76} \sim \frac{13}{47}$

Table 2: Table for the limit divergence of $\alpha_0 = [3] = 1/(3 + \tau^{-1}) \simeq 0.2764$ ($360\alpha_0 \simeq 99.5^\circ$). The parastichy pairs are generated from the seed pair (1, 3) by a Fibonacci recurrence relation. The sequence 1,3,4,7,11,... is called the Lucas sequence or the first accessory sequence.

indicates $\frac{1}{3} < \alpha_0 < \frac{1}{2}$. As an example, let us take a fraction $\alpha = \frac{21}{76}$. It is found in the eighth column of Table 2, from which the conditions $47 \leq n_c < 76$ and $\frac{8}{29} < \alpha_0 < \frac{13}{47}$ are read. These results are used in the next section (Table 20).

The tables show that the denominator of a fraction α and the parastichy numbers are correlated with the threshold numbers for n_c . The numbers comprise a characteristic sequence of integers. The main sequence in Table 1 is characterized with the Fibonacci sequence of 1, 2, 3, 5, 8, 13, 21, ..., while Table 6 has a sequence of 1, 2, 3, 2, 5, 7, 12, 19, ..., which is sometimes called the lateral sequence. Three consecutive numbers of a sequence satisfy the Fibonacci recurrence relation ($2 + 5 = 7$, $5 + 7 = 12$, $7 + 12 = 19$), except for the first several numbers (like 1, 2, 3 in the lateral sequence). Therefore, each phyllotactic sequence is referred to by a pair of seed integers for the Fibonacci recurrence formula. The seed pair of each table, such as (2, 5) in Table 6, is highlighted in boldface.

α	$\frac{1}{4}$	$\frac{1}{5}$	$\frac{2}{9}$	$\frac{3}{14}$	$\frac{5}{23}$	$\frac{8}{37}$	$\frac{13}{60}$	$\frac{21}{97}$
	(1,3)	(1,4)	(4,5)	(5,9)	(9,14)	(14,23)	(23,37)	(37,60)
n_c	3~	4~	5~	9~	14~	23~	37~	60~
α_0	$0 \sim \frac{1}{3}$	$0 \sim \frac{1}{4}$	$\frac{1}{5} \sim \frac{1}{4}$	$\frac{1}{5} \sim \frac{2}{9}$	$\frac{3}{14} \sim \frac{2}{9}$	$\frac{3}{14} \sim \frac{5}{23}$	$\frac{8}{37} \sim \frac{5}{23}$	$\frac{8}{37} \sim \frac{13}{60}$

Table 3: Table for the limit divergence of $\alpha_0 = [4] = 1/(4+\tau^{-1}) \simeq 0.2165$ ($360\alpha_0 \simeq 78.0^\circ$). The parastichy pairs except (1,3) are generated from the seed pair (1,4) by a Fibonacci recurrence relation. The sequence 1,4,5,9,14,... is called the second accessory sequence.

α	$\frac{1}{4}$	$\frac{1}{5}$	$\frac{1}{6}$	$\frac{2}{11}$	$\frac{3}{17}$	$\frac{5}{28}$	$\frac{8}{45}$	$\frac{13}{73}$
	(1,3)	(1,4)	(1,5)	(5,6)	(6,11)	(11,17)	(17,28)	(28,45)
n_c	3~	4~	5~	6~	11~	17~	28~	45~
α_0	$0 \sim \frac{1}{3}$	$0 \sim \frac{1}{4}$	$0 \sim \frac{1}{5}$	$\frac{1}{6} \sim \frac{1}{5}$	$\frac{1}{6} \sim \frac{2}{11}$	$\frac{3}{17} \sim \frac{2}{11}$	$\frac{3}{17} \sim \frac{5}{28}$	$\frac{8}{45} \sim \frac{5}{28}$

Table 4: $\alpha_0 = [5] = 1/(5+\tau^{-1}) \simeq 0.1780$ ($360\alpha_0 \simeq 64.1^\circ$).

α	$\frac{1}{4}$	$\frac{1}{5}$	$\frac{1}{6}$	$\frac{1}{7}$	$\frac{2}{13}$	$\frac{3}{20}$	$\frac{5}{33}$	$\frac{8}{53}$
	(1,3)	(1,4)	(1,5)	(1,6)	(6,7)	(7,13)	(13,20)	(20,33)
n_c	3~	4~	5~	6~	7~	13~	20~	33~
α_0	$0 \sim \frac{1}{3}$	$0 \sim \frac{1}{4}$	$0 \sim \frac{1}{5}$	$0 \sim \frac{1}{6}$	$\frac{1}{7} \sim \frac{1}{6}$	$\frac{1}{7} \sim \frac{2}{13}$	$\frac{3}{20} \sim \frac{2}{13}$	$\frac{3}{20} \sim \frac{5}{33}$

Table 5: $\alpha_0 = [6] = 1/(6+\tau^{-1}) \simeq 0.15112$ ($360\alpha_0 \simeq 54.4^\circ$).

α	$\frac{2}{5}$	$\frac{3}{7}$	$\frac{5}{12}$	$\frac{8}{19}$	$\frac{13}{31}$	$\frac{21}{50}$	$\frac{34}{81}$	$\frac{55}{131}$
	(2,3)	(2,5)	(5,7)	(7,12)	(12,19)	(19,31)	(31,50)	(50,81)
n_c	3~	5~	7~	12~	19~	31~	50~	81~
α_0	$\frac{1}{3} \sim \frac{1}{2}$	$\frac{2}{5} \sim \frac{1}{2}$	$\frac{2}{5} \sim \frac{3}{7}$	$\frac{5}{12} \sim \frac{3}{7}$	$\frac{5}{12} \sim \frac{8}{19}$	$\frac{13}{31} \sim \frac{8}{19}$	$\frac{13}{31} \sim \frac{21}{50}$	$\frac{34}{81} \sim \frac{21}{50}$

Table 6: $\alpha_0 = [2, 2] = 1/(2+1/(2+\tau^{-1})) \simeq 0.4198$ ($360\alpha_0 \simeq 151.1^\circ$). The parastichy pairs except (2,3) are generated from the seed pair (2,5). The sequence 2,5,7,12,19,... is called the first lateral sequence.

α	$\frac{1}{4}$ (1,3)	$\frac{2}{7}$ (3,4)	$\frac{3}{10}$ (3,7)	$\frac{5}{17}$ (7,10)	$\frac{8}{27}$ (10,17)	$\frac{13}{44}$ (17,27)	$\frac{21}{71}$ (27,44)	$\frac{34}{115}$ (44,71)
n_c	3~	4~	7~	10~	17~	27~	44~	71~
α_0	$0 \sim \frac{1}{3}$	$\frac{1}{4} \sim \frac{1}{3}$	$\frac{2}{7} \sim \frac{1}{3}$	$\frac{2}{7} \sim \frac{3}{10}$	$\frac{5}{17} \sim \frac{3}{10}$	$\frac{5}{17} \sim \frac{8}{27}$	$\frac{13}{44} \sim \frac{8}{27}$	$\frac{13}{44} \sim \frac{21}{71}$

Table 7: $\alpha_0 = [3, 2] = 1/(3 + 1/(2 + \tau^{-1})) \simeq 0.2957$ ($360\alpha_0 \simeq 106.4^\circ$).

α	$\frac{2}{5}$ (2,3)	$\frac{3}{7}$ (2,5)	$\frac{4}{9}$ (2,7)	$\frac{7}{16}$ (7,9)	$\frac{11}{25}$ (9,16)	$\frac{18}{41}$ (16,25)	$\frac{29}{66}$ (25,41)	$\frac{47}{107}$ (41,66)
n_c	3~	5~	7~	9~	16~	25~	41~	66~
α_0	$\frac{1}{3} \sim \frac{1}{2}$	$\frac{2}{5} \sim \frac{1}{2}$	$\frac{3}{7} \sim \frac{1}{2}$	$\frac{3}{7} \sim \frac{4}{9}$	$\frac{7}{16} \sim \frac{4}{9}$	$\frac{7}{16} \sim \frac{11}{25}$	$\frac{18}{41} \sim \frac{11}{25}$	$\frac{18}{41} \sim \frac{29}{66}$

Table 8: $\alpha_0 = [2, 3] = 1/(2 + 1/(3 + \tau^{-1})) \simeq 0.4393$ ($360\alpha_0 \simeq 158.1^\circ$). The sequence 2,7,9,16,... is called the second lateral sequence.

α	$\frac{2}{7}$ (3,4)	$\frac{3}{10}$ (3,7)	$\frac{4}{13}$ (3,10)	$\frac{7}{23}$ (10,13)	$\frac{11}{36}$ (13,23)	$\frac{18}{59}$ (23,36)	$\frac{29}{95}$ (36,59)	$\frac{47}{154}$ (59,95)
n_c	4~	7~	10~	13~	23~	36~	59~	95~
α_0	$\frac{1}{4} \sim \frac{1}{3}$	$\frac{2}{7} \sim \frac{1}{3}$	$\frac{3}{10} \sim \frac{1}{3}$	$\frac{3}{10} \sim \frac{4}{13}$	$\frac{7}{23} \sim \frac{4}{13}$	$\frac{7}{23} \sim \frac{11}{36}$	$\frac{18}{59} \sim \frac{11}{36}$	$\frac{18}{59} \sim \frac{29}{95}$

Table 9: $\alpha_0 = [3, 3] = 1/(3 + 1/(3 + \tau^{-1})) \simeq 0.3052$ ($360\alpha_0 \simeq 109.9^\circ$).

α	$\frac{1}{4}$ (1,3)	$\frac{1}{5}$ (1,4)	$\frac{2}{9}$ (4,5)	$\frac{3}{13}$ (4,9)	$\frac{5}{22}$ (9,13)	$\frac{8}{35}$ (13,22)	$\frac{13}{57}$ (22,35)	$\frac{21}{92}$ (35,57)
n_c	3~	4~	5~	9~	13~	22~	35~	57~
α_0	$0 \sim \frac{1}{3}$	$0 \sim \frac{1}{4}$	$\frac{1}{5} \sim \frac{1}{4}$	$\frac{2}{9} \sim \frac{1}{4}$	$\frac{2}{9} \sim \frac{3}{13}$	$\frac{5}{22} \sim \frac{3}{13}$	$\frac{5}{22} \sim \frac{8}{35}$	$\frac{13}{57} \sim \frac{8}{35}$

Table 10: $\alpha_0 = [4, 2] = 1/(4 + 1/(2 + \tau^{-1})) \simeq 0.2282$ ($360\alpha_0 \simeq 82.2^\circ$).

α	$\frac{2}{5}$ (2,3)	$\frac{3}{8}$ (3,5)	$\frac{4}{11}$ (3,8)	$\frac{7}{19}$ (8,11)	$\frac{11}{30}$ (11,19)	$\frac{18}{49}$ (19,30)	$\frac{29}{79}$ (30,49)	$\frac{47}{128}$ (49,79)
n_c	3~	5~	8~	11~	19~	30~	49~	79~
α_0	$\frac{1}{3} \sim \frac{1}{2}$	$\frac{1}{3} \sim \frac{2}{5}$	$\frac{1}{3} \sim \frac{3}{8}$	$\frac{4}{11} \sim \frac{3}{8}$	$\frac{4}{11} \sim \frac{7}{19}$	$\frac{11}{30} \sim \frac{7}{19}$	$\frac{11}{30} \sim \frac{18}{49}$	$\frac{29}{79} \sim \frac{18}{49}$

Table 11: $\alpha_0 = [2, 1, 2] = 1/(2 + 1/(1 + 1/(2 + \tau^{-1}))) \simeq 0.3672$ ($360\alpha_0 \simeq 132.2^\circ$).

α	$\frac{2}{5}$ (2,3)	$\frac{3}{7}$ (2,5)	$\frac{5}{12}$ (5,7)	$\frac{7}{17}$ (5,12)	$\frac{12}{29}$ (12,17)	$\frac{19}{46}$ (17,29)	$\frac{31}{75}$ (29,46)	$\frac{50}{121}$ (46,75)
n_c	3~	5~	7~	12~	17~	29~	46~	75~
α_0	$\frac{1}{3} \sim \frac{1}{2}$	$\frac{2}{5} \sim \frac{1}{2}$	$\frac{2}{5} \sim \frac{3}{7}$	$\frac{2}{5} \sim \frac{5}{12}$	$\frac{7}{17} \sim \frac{5}{12}$	$\frac{7}{17} \sim \frac{12}{29}$	$\frac{19}{46} \sim \frac{12}{29}$	$\frac{19}{46} \sim \frac{31}{75}$

Table 12: $\alpha_0 = [2, 2, 2] = 1/(2 + 1/(2 + 1/(2 + \tau^{-1}))) \simeq 0.4133$ ($360\alpha_0 \simeq 148.8^\circ$).

α	$\frac{1}{4}$ (1,3)	$\frac{2}{7}$ (3,4)	$\frac{3}{11}$ (4,7)	$\frac{4}{15}$ (4,11)	$\frac{7}{26}$ (11,15)	$\frac{11}{41}$ (15,26)	$\frac{18}{67}$ (26,41)	$\frac{29}{108}$ (41,67)
n_c	3~	4~	7~	11~	15~	26~	41~	67~
α_0	$0 \sim \frac{1}{3}$	$\frac{1}{4} \sim \frac{1}{3}$	$\frac{1}{4} \sim \frac{2}{7}$	$\frac{1}{4} \sim \frac{3}{11}$	$\frac{4}{15} \sim \frac{3}{11}$	$\frac{4}{15} \sim \frac{7}{26}$	$\frac{11}{41} \sim \frac{7}{26}$	$\frac{11}{41} \sim \frac{18}{67}$

Table 13: $\alpha_0 = [3, 1, 2] = 1/(3 + 1/(1 + 1/(2 + \tau^{-1}))) \simeq 0.2686$ ($360\alpha_0 \simeq 96.7^\circ$).

α	$\frac{1}{4}$ (1,3)	$\frac{2}{7}$ (3,4)	$\frac{3}{10}$ (3,7)	$\frac{5}{17}$ (7,10)	$\frac{7}{24}$ (7,17)	$\frac{12}{41}$ (17,24)	$\frac{19}{65}$ (24,41)	$\frac{31}{106}$ (41,65)
n_c	3~	4~	7~	10~	17~	24~	41~	65~
α_0	$0 \sim \frac{1}{3}$	$\frac{1}{4} \sim \frac{1}{3}$	$\frac{2}{7} \sim \frac{1}{3}$	$\frac{2}{7} \sim \frac{5}{17}$	$\frac{2}{7} \sim \frac{5}{17}$	$\frac{7}{24} \sim \frac{5}{17}$	$\frac{7}{24} \sim \frac{12}{41}$	$\frac{19}{65} \sim \frac{12}{41}$

Table 14: $\alpha_0 = [3, 2, 2] = 1/(3 + 1/(2 + 1/(2 + \tau^{-1}))) \simeq 0.2924$ ($360\alpha_0 \simeq 105.3^\circ$).

α	$\frac{2}{5}$ (2,3)	$\frac{3}{8}$ (3,5)	$\frac{4}{11}$ (3,8)	$\frac{5}{14}$ (3,11)	$\frac{9}{25}$ (11,14)	$\frac{14}{39}$ (14,25)	$\frac{23}{64}$ (25,39)	$\frac{37}{103}$ (39,64)
n_c	3~	5~	8~	11~	14~	25~	39~	64~
α_0	$\frac{1}{2} \sim \frac{1}{3}$	$\frac{1}{3} \sim \frac{2}{5}$	$\frac{1}{3} \sim \frac{3}{8}$	$\frac{1}{3} \sim \frac{4}{11}$	$\frac{5}{14} \sim \frac{4}{11}$	$\frac{5}{14} \sim \frac{9}{25}$	$\frac{14}{39} \sim \frac{9}{25}$	$\frac{14}{39} \sim \frac{23}{64}$

Table 15: $\alpha_0 = [2, 1, 3] = 1/(2 + 1/(1 + 1/(3 + \tau^{-1}))) \simeq 0.3593$ ($360\alpha_0 \simeq 129.3^\circ$).

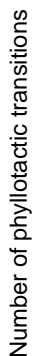
α	$\frac{2}{5}$	$\frac{3}{7}$	$\frac{4}{9}$	$\frac{7}{16}$	$\frac{10}{23}$	$\frac{17}{39}$	$\frac{27}{62}$	$\frac{44}{101}$
	(2,3)	(2,5)	(2,7)	(7,9)	(7,16)	(16,23)	(23,39)	(39,62)
n_c	3~	5~	7~	9~	16~	23~	39~	62~
α_0	$\frac{1}{3} \sim \frac{1}{2}$	$\frac{2}{5} \sim \frac{1}{2}$	$\frac{3}{7} \sim \frac{1}{2}$	$\frac{3}{7} \sim \frac{4}{9}$	$\frac{3}{7} \sim \frac{7}{16}$	$\frac{10}{23} \sim \frac{7}{16}$	$\frac{10}{23} \sim \frac{17}{39}$	$\frac{27}{62} \sim \frac{17}{39}$

Table 16: $\alpha_0 = [2, 3, 2] = 1/(2 + 1/(3 + 1/(2 + \tau^{-1}))) \simeq 0.4356$ ($360\alpha_0 \simeq 156.8^\circ$).

α	$\frac{2}{5}$	$\frac{3}{7}$	$\frac{5}{12}$	$\frac{7}{17}$	$\frac{9}{22}$	$\frac{16}{39}$	$\frac{25}{61}$	$\frac{41}{100}$
	(2,3)	(2,5)	(5,7)	(5,12)	(5,17)	(17,22)	(22,39)	(39,61)
n_c	3~	5~	7~	12~	17~	22~	39~	61~
α_0	$\frac{1}{3} \sim \frac{1}{2}$	$\frac{2}{5} \sim \frac{1}{2}$	$\frac{2}{5} \sim \frac{3}{7}$	$\frac{2}{5} \sim \frac{5}{12}$	$\frac{2}{5} \sim \frac{7}{17}$	$\frac{9}{22} \sim \frac{7}{17}$	$\frac{9}{22} \sim \frac{16}{39}$	$\frac{25}{61} \sim \frac{16}{39}$

Table 17: $\alpha_0 = [2, 2, 3] = 1/(2 + 1/(2 + 1/(3 + \tau^{-1}))) \simeq 0.4100$ ($360\alpha_0 \simeq 147.6^\circ$).

Having prepared the mathematical relationship between the initial divergence α_0 , the final divergence α and the trace length n_c , we are in a position to give an account of what is special about the golden angle. As shown below in Figs. 16 and 19, discontinuous change in phyllotactic fraction α , or phyllotactic transition, involves reconstruction of the vascular structure. Therefore, it is advantageous for a plant to suppress the transitions as few as possible. As internodes vary in length during growth, the trace length per internode n_c may change accordingly. For instance, n_c may depend on the plastochron ratio a (Appendix A). Patterns with a fraction that appears in many places of Fig. 7 are stable against occasional changes in n_c . The lowest fraction that appears more than once is $\frac{2}{5}$. Thus, systems with initial divergence angle giving rise to stable fractions are most likely to survive. Among all possible values of α_0 , the initial divergence angle which suffers the least number of phyllotactic transitions is the golden angle $\alpha_0 = [2]$ (137.5 degrees). This is a summary of the evolutionary mechanism for the golden angle (Okabe (2011)). Fig. 8 shows phyllotactic fractions resulting from various representative values of α_0 while n_c increases up to eleven. The number of phyllotactic transitions is indicated by a dashed line. In this example, initial divergence angles from 135° to 154° are most likely to be naturally selected.



27

α	$\frac{2}{5}$ (2,3)	$\frac{3}{8}$ (3,5)	$\frac{5}{13}$ (5,8)	$\frac{7}{18}$ (5,13)	$\frac{12}{31}$ (13,18)	$\frac{19}{49}$ (18,31)	$\frac{31}{80}$ (31,49)	$\frac{50}{129}$ (49,80)
n_c	3 \sim	5 \sim	8 \sim	13 \sim	18 \sim	31 \sim	49 \sim	80 \sim
α_0	$\frac{1}{3} \sim \frac{1}{2}$	$\frac{1}{3} \sim \frac{2}{5}$	$\frac{3}{8} \sim \frac{2}{5}$	$\frac{5}{13} \sim \frac{2}{5}$	$\frac{5}{13} \sim \frac{7}{18}$	$\frac{12}{31} \sim \frac{7}{18}$	$\frac{12}{31} \sim \frac{19}{49}$	$\frac{31}{80} \sim \frac{19}{49}$

Table 18: $\alpha_0 = [2, 1, 1, 2] = 1/(2 + 1/(1 + 1/(1 + 1/(2 + \tau^{-1})))) \simeq 0.3876$ ($360\alpha_0 \simeq 139.5^\circ$).

α	$\frac{1}{4}$ (1,3)	$\frac{1}{5}$ (1,4)	$\frac{1}{6}$ (1,5)	$\frac{1}{7}$ (1,6)	$\frac{2}{13}$ (6,7)	$\frac{3}{19}$ (6,13)	$\frac{5}{32}$ (13,19)	$\frac{8}{51}$ (19,32)
n_c	3 \sim	4 \sim	5 \sim	6 \sim	7 \sim	13 \sim	19 \sim	32 \sim
α_0	$0 \sim \frac{1}{3}$	$0 \sim \frac{1}{4}$	$0 \sim \frac{1}{5}$	$0 \sim \frac{1}{6}$	$\frac{2}{13} \sim \frac{1}{6}$	$\frac{2}{13} \sim \frac{3}{19}$	$\frac{5}{32} \sim \frac{3}{19}$	$\frac{5}{32} \sim \frac{8}{51}$

Table 19: $\alpha_0 = [6, 2] = 1/(6 + 1/(2 + \tau^{-1})) \simeq 0.1567$ ($360\alpha_0 \simeq 56.4^\circ$).

3. Precision of initial divergence angle

As the evolutionary mechanism relies on statistical screening processes, it does not predict a limit divergence angle with unlimited precision. It is an empirical fact that divergence angles at the level of the shoot apex are regulated toward a mean value comparable with an ideal angle given by the formula (2) after some transient fluctuations (Davies (1939); Snow and Snow (1962); Barabé et al. (2010)). Excepting initial fluctuations, the precision with which leaves are organized on the apical meristems is remarkable. It is undoubtedly controlled by genetics, though it may be slightly affected by light stimuli depending on the orientation (Kumazawa and Kumazawa (1971)). Twenty samples of young shoots of *Erigeron sumatrensis* (Sumatran fleabane) show mean divergence angles from 137.23° to 137.97° with the sample average of $137.499 \pm 0.212^\circ$ (Kumazawa and Kumazawa (1971)). The mean divergence angle of the individual plant may deviate statistically significantly from the ideal limit angle (Maksymowych and Erickson (1977)). Sometimes there occur other ideal divergence angles than the normal golden angle of 137.5° . Phyllotaxis of *Musa sapientum* (banana) changes with the age of the plant from $\frac{2}{5}$ through $\frac{3}{7}$ to $\frac{4}{9}$ (Skutch (1927)). This is consistent with a unique initial divergence of $\alpha_0 = [2, 3]$ (Table 8), which seems to be true for all species of *Musa* propagated vegetatively. Rutishauser (1998) has presented a remarkably exotic pattern of *Picea abies* (Norway spruce) showing a (6, 13) phyllotaxis (Table 19).

The evolutionary mechanism predicts a correlation between the range of values of the initial divergence α_0 and the highest-order fraction α attained in evolutionary or phylogenetic processes. The correlation may seem strange at first glance, as it appears as an advanced correlation in developmental or ontogenetic processes of a plant; the precision of divergence angles on a young shoot is determined by the phyllotactic form at its maturity. This phylogenetic correlation is contrasted with the instantaneous correlation that causal models predict between the divergence angle and parastichies of the standing pattern. In general, divergence angles of a (3, 5) phyllotaxis are widely variable within $\frac{1}{3} < \alpha_0 < \frac{2}{5}$, whereas the range is narrowed to $\frac{3}{8} < \alpha_0 < \frac{2}{5}$ when the parastichy pair is raised to (5, 8). Remark that these are general results drawn from regularity of phyllotactic patterns. The ranges may be restricted further depending on specific assumptions of models. For instance, consider a regular pattern with a parastichy pair (1, 2), which is realized for any value of divergence angle. According to Schwendener's model, however, (1, 2) patterns for $0 < \alpha_0 < 0.36$, i.e., from 0 to 128.6 degrees, are not realized, for a transition to a (2, 3) phyllotaxis intervenes at $\alpha_0 = 0.36$ (Adler (1974); Levitov (1991); Douady and Couder (1996)). See the top branch of the zigzag path in Fig. 2. The threshold angle $\alpha_0 = 0.36$ specifically depends on geometrical assumptions, e.g. the circular shape of 'leaves' on the stem cylinder surface. Accordingly, the divergence angles for the parastichy pair (1, 2) is predicted to vary continuously within $0.36 < \alpha_0 < \frac{1}{2}$, i.e., from 128.6° to 180°. The range is narrowed substantially but still so wide that it is incompatible with observations that divergence angles are very close to 137.5° even in systems of low phyllotaxis. Causal models attain a target pattern with 137.5° by way of an almost opposite (1, 2) pattern with divergence of about 180°. Therefore, they cannot but allow the wide latitude of divergence angles for the (1, 2) pattern, in disagreement with precise control of actual systems (cf. Fig. 12(a)). This is a very old problem which van Iterson (1907) (p. 247) was well aware of. Nonetheless, it has been left unnoticed despite a marginal rise of various causal models in recent years. With reference to experimental evidence, Church (1904) (p. 340) remarks that already at a (2, 3) system the ideal angle is attained within an error of about one degree. The present model explains the non-correspondence between divergence angle α_0 and parastichy numbers by relating the allowed range of α_0 not with the parastichy numbers but with the highest order fraction α that the plant would attain in its mature state.

By measuring initial divergence angles for thirty species of plants, Fujita

(1939) found that frequency distributions of the divergence angles are almost independent of the parastichy numbers. The divergence angles cluster in a narrow range. The width of the range quantifies the remarkable constancy of the divergence angle (Fig. 12(a)). This results look puzzling from a causal viewpoint (Jean (1986, 1994)). By contrast, they are consistent with the evolutionary mechanism in that the initial angle α_0 is independent of the parastichy numbers. According to Fujita (1939), initial divergence angles for the main sequence fall within $138 \pm 7^\circ$ (Fujita (1939)), irrespective of the parastichy pair. This corresponds to $\frac{3}{8} < \alpha_0 < \frac{2}{5}$ (135 to 144 degrees), which is as expected for the highest-order fraction of $\alpha = \frac{5}{13}$ (Table 1). Similarly, an estimate of $99 \pm 4^\circ$ for *Cunninghamia lanceolata* (China fir) (Fujita (1939)) is consistent with $\frac{1}{4} < \alpha_0 < \frac{2}{7}$ for $\alpha = \frac{3}{11}$ in Table 2, and a narrow scattering of $151 \pm 3^\circ$ for (2, 5) phyllotaxis at the apex of *Cephalotaxus drupacea* (Japanese plum yew) (Fujita (1937)) is consistent with $\frac{5}{12} < \alpha_0 < \frac{3}{7}$ for $\alpha = \frac{8}{19}$ (Table 6).

Let us make a general remark that parastichy does not substitute for divergence angle. The former depends on size and shape of the pattern unit or on a radial or internodal length scale. Therefore, several different parastichy pairs may be arbitrarily related to a single divergence angle. Parastichy numbers given in Tables 1~18 are the simplest pairs, which normally represent contact parastichies.

Large fluctuations in the initial divergence α_0 may cause the phyllotactic transition in the vascular structure, even if the trace length n_c is fixed constant. To suppress the transition that could happen, the divergence α_0 has to be restricted within one of the ranges determined by n_c . For a fixed length of $n_c = 5$, the fraction α is plotted against the initial divergence α_0 in Fig. 9. To maintain a $\frac{3}{8}$ phyllotaxis, the initial divergence α_0 must stay within $\frac{1}{3} < \alpha_0 < \frac{2}{5}$ (from 120° to 144°); otherwise one would observe occasional excursions to $\frac{2}{7}$ (for $\alpha_0 < \frac{1}{3}$) or $\frac{3}{7}$ (for $\frac{2}{5} < \alpha_0$) in the midst of a steady course of the $\frac{3}{8}$ phyllotaxis. Similarly, to maintain a $\frac{5}{13}$ phyllotaxis, the initial divergence α_0 has to be kept within $\frac{3}{8} < \alpha_0 < \frac{2}{5}$ (from 135° to 144°); otherwise one would find $\frac{4}{11}$ (for $\alpha_0 < \frac{3}{8}$) or $\frac{5}{12}$ (for $\frac{2}{5} < \alpha_0$) within the mature state of the $\frac{5}{13}$ phyllotaxis (cf. Fig. 8). Thus, it is explained why the initial divergence angle has to be ‘quantized’ or fixed around a special constant with precision determined by the length of leaf traces. For this mechanism to work, stepwise changes in the fraction α of the vascular order, which are presumed to occur if the initial divergence angle α_0 were not optimum, should incur penalties of extra energy. Thus, efficiency of the mechanism depends on the energy cost per transition, which should depend on species. By and

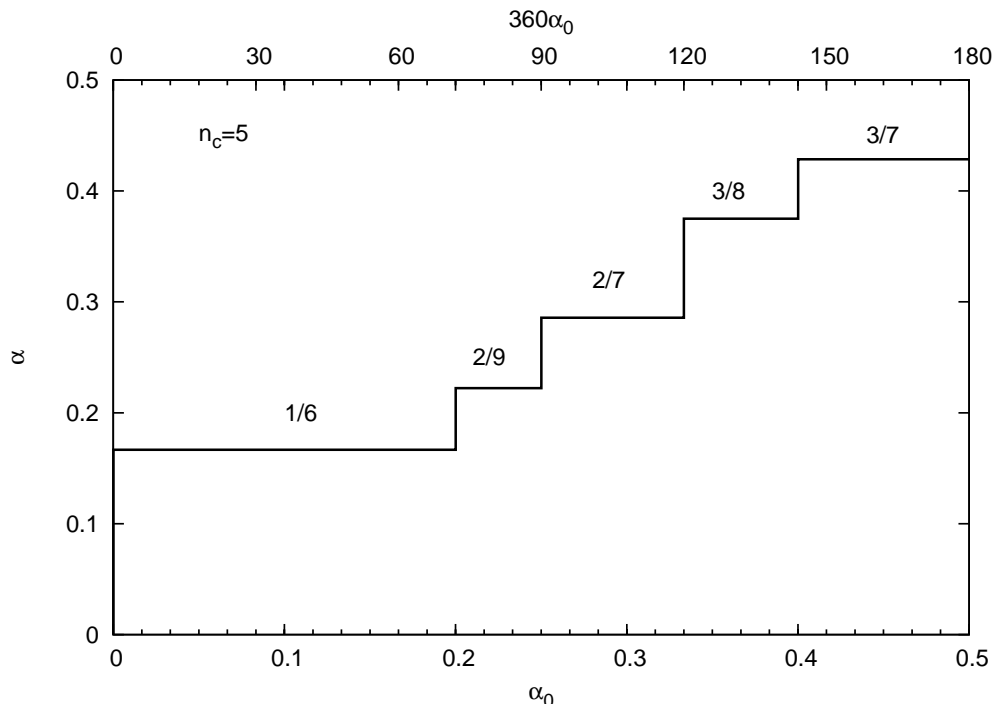


Figure 9: Phyllotactic fraction α versus initial divergence angle α_0 for a fixed length $n_c = 5$ of leaf traces. The fractional order changes discontinuously while α_0 changes continuously. There are plateaus for five phyllotactic orders with $\frac{1}{6}$, $\frac{2}{9}$, $\frac{2}{7}$, $\frac{3}{8}$ and $\frac{3}{7}$. The initial divergence α_0 is ‘quantized’ within a plateau to avoid the discontinuous transition. In other words, leaves are initiated regularly with a given angular precision. The wide plateau for $\alpha = \frac{1}{6}$ is the most unstable against changes in n_c , while the plateau at $\alpha = \frac{3}{8}$ is the most stable.

large, however, the number of transition may be used as a good measure of the total cost, at least as a first approximation (Fig. 8).

4. Fossil record and diversity of phyllotaxis

Dickson (1871) found that nine among thirteen specimens of fossil remains of *Lepidodendron* (scale tree) show helical phyllotaxis, of which only three belong to the main sequence. This is in striking contrast to the current dominance of the main sequence in existing species (Fujita (1938); Zagórska-Marek (1985); Jean (1994)). Therefore, Dickson concluded that the phyllotaxis of

No.	1	2	3	8	9,10	11	12	13
α	$\frac{13}{34}$ (13,21)	$\frac{21}{55}$ (21,34)	$\frac{55}{144}$ (55,89)	$\frac{21}{76}$ (29,47)	$\frac{13}{60}$ (23,37)	$\frac{21}{50}$ (19,31)	$\frac{18}{59}$ (23,36)	$\frac{47}{154}$ (59,95)
n_c	[21, 34]	[34,55]	[89,144]	[47,76]	[37,60]	[31,50]	[36,59]	[95,154]
α_0	$\frac{8}{21} \sim \frac{5}{13}$ [2]	$\frac{8}{21} \sim \frac{13}{34}$ [2]	$\frac{21}{55} \sim \frac{34}{89}$ [2]	$\frac{8}{29} \sim \frac{13}{47}$ [3]	$\frac{8}{37} \sim \frac{5}{23}$ [4]	$\frac{13}{31} \sim \frac{8}{19}$ [2,2]	$\frac{7}{23} \sim \frac{11}{36}$ [3,3]	$\frac{18}{59} \sim \frac{29}{95}$ [3,3]

Table 20: Ranges of n_c and α_0 for the phyllotactic fraction α and the contact parastichy pair (n, m) of the nine specimens of *Lepidodendron* by Dickson (1871). Abbreviations [21, 34] and $\frac{8}{21} \sim \frac{5}{13}$ mean $21 \leq n_c < 34$ and $\frac{8}{21} < \alpha_0 < \frac{5}{13}$. The bracket notation in (2) is used for the limit divergence in the last row. Only the first three specimens belong to the main sequence $\alpha_0 = [2]$ (137.5°).

Lepidodendron is extremely variable, as much so as that of those most variable plants like cacti. His results provide us with important information when they are analyzed in terms of the model.

In the second and third line of Table 20, the phyllotactic fractions and the parastichy pairs for the nine specimens are presented after Dickson. The fourth and fifth line are the corresponding ranges of n_c and α_0 according to Tables 1, 2, 3, 6, and 9. The last line is the limit divergence in terms of the bracket notation defined by (2) in the last section. For instance, in the second column, the specimen No. 1 has a $\frac{13}{34}$ phyllotaxis ($\alpha = \frac{13}{34}$) with the parastichy pair of (13, 21), for which $21 \leq n_c < 34$ and $\frac{8}{21} < \alpha_0 < \frac{5}{13}$. The limit divergence of $\alpha_0 = [2]$ (137.5°) satisfies the latter condition. The specimens Nos. 1-3 belong to the main sequence $\alpha_0 = [2]$. Fig. 10(a) represents graphically the parameter regions allowed for n_c and α_0 . By comparison, Fig. 10(b) gives a theoretical result for the most favored regions in which the number of phyllotactic transitions is minimal (Okabe (2011)).

According to Fig. 10(a), the trace length n_c appears to be independent of the initial divergence α_0 . Moreover, n_c is not as variable as α_0 . As the order of phyllotaxis is very high, there is considerable uncertainty in n_c , while α_0 is quite accurate. The specimens may be divided into two groups in terms of n_c , i.e., one with $n_c \sim 50$ and the other with $n_c > 100$. The fact that the fossil specimens show various but accurate values of α_0 strongly suggests the evolutionary origin of the special divergence angles. It is impossible to tabulate all phyllotactic fractions for such a large value as $n_c = 50$ due to lack of space, but it is mentioned only that the number of possible phyllotactic fractions at $n_c = 50$ amounts to $387 (\simeq 3n_c^2/\pi^2/2)$. Among them, only the single

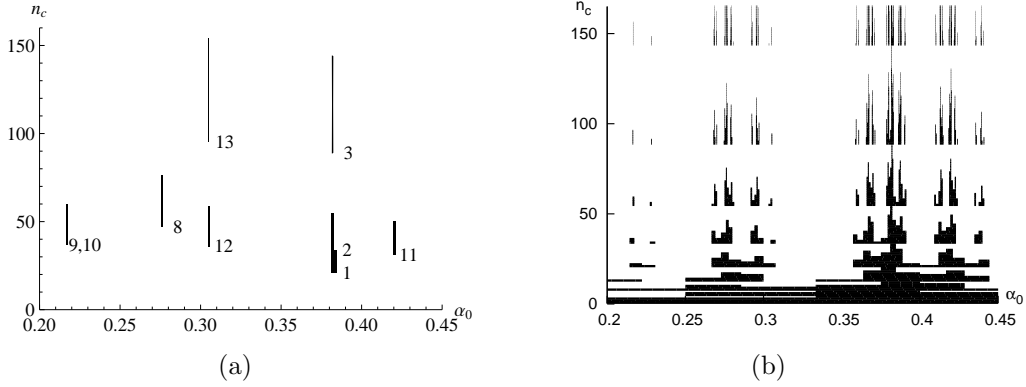


Figure 10: (a) Ranges of α_0 and n_c for the specimens of Dickson (1871) (Table 20) are painted black in the α_0 - n_c plane. (b) A theoretical result for the regions in which the number of phyllotactic transitions is minimal (adapted from Fig. 13 of Okabe (2011)). The golden angle $\alpha_0 \simeq 0.382$ (137.5°) is singled out for n_c below Fibonacci numbers such as 34, 55, 89 and 144.

fraction $\alpha = \frac{21}{55}$ of the main sequence falls in the optimum regions depicted in Fig. 10(b), while the specimens Nos. 8-12 do not meet the optimum condition. Nevertheless, all the reported specimens possess the irrational numbers expressed in the form of (2), as expected in the evolutionary mechanism (cf. Table 2 of Okabe (2011)). Phyllotactic patterns for $\alpha_0 = [3, 2]$, $[2, 3]$, $[2, 1, 2]$ and others are not reported, presumably because of lack of enough samples. Thus, anomalous patterns are regarded as relics of evolutionary processes.

It has been an unresolved problem in what quantitative terms normal and anomalous phyllotaxis are differentiated. The number of phyllotactic transition during a steady growth provides us with a numerical measure of relative fitness in evolution. The most fit divergence angles are indicated in Fig. 10(b). They are peaks of a ‘fitness landscape’ (Niklas (1997)), shown in Fig. 11 (Okabe (2011)). A close inspection of the frequency distribution curves of Fujita (1939) indicates that a primary peak accompanies small subsidiary peaks at anomalous angles. In Fig. 12, Fujita’s result for *Lysimachia clethroides* (gooseneck loosestrife) is arranged along with transections of the fitness landscape in Fig. 11. Roberts (1984) has discussed that his chemical contact pressure model explains the anomalous subsidiary peaks. However, his conclusion is based on circular reasoning that anomalous systems are less frequent because they are anomalous. Similar fitness curves are obtained for light absorption efficiency of rosette plants (Niklas (1988, 1998);

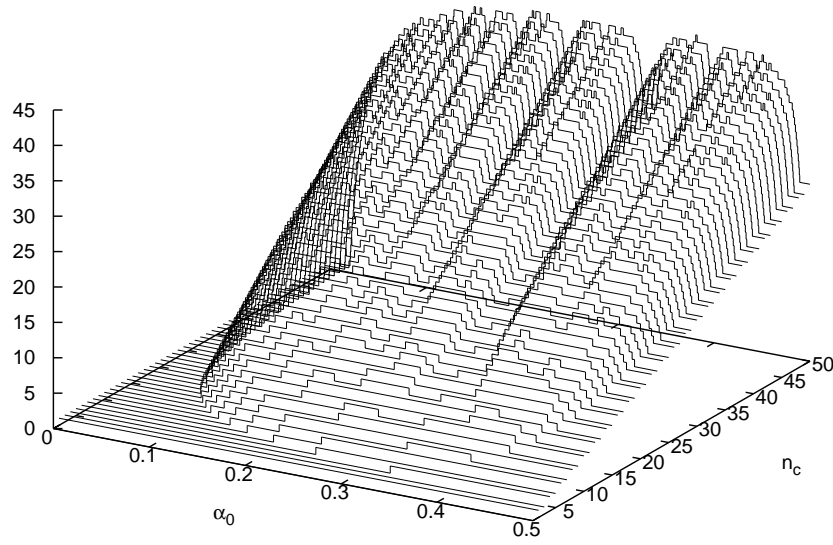


Figure 11: Three-dimensional fitness landscape. The vertical axis representing ‘fitness’ is n_c minus the number of phyllotactic transition. The variables on the base plane are α_0 and n_c . The number of transition increases with n_c . The fitness has a flat bottom minimum in the worst case of $\alpha_0 \simeq 0$, whereas there are ‘fitness peaks’ at $\alpha_0 = [2] \simeq 0.38$ (the main sequence), $\alpha_0 = [3] \simeq 0.28$ (an accessory sequence) and others, whose widths decrease as n_c increases (Okabe (2011)).

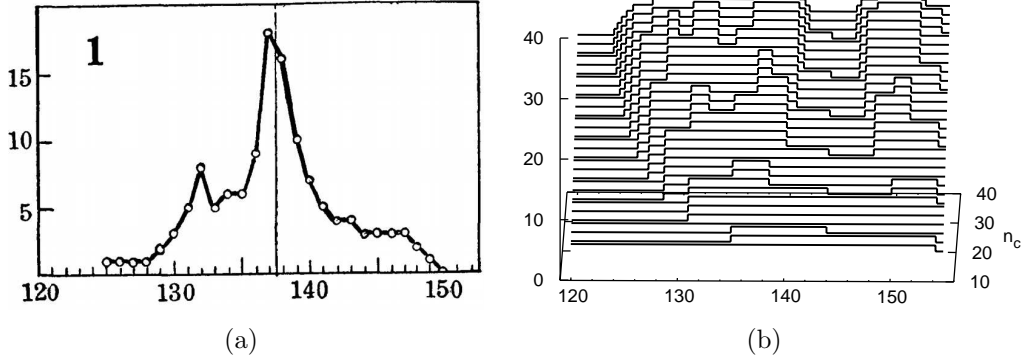


Figure 12: (a) Frequency distribution of initial divergence angles for a (1, 2) phyllotaxis of *Lysimachia clethroides* by Fujita (1939). (b) An enlarged view of a relative ‘fitness’ in Fig. 11 is plotted against the divergence angle in degrees, $360\alpha_0$. The peak plateau extends from 135 to 144 degrees at $n_c = 12$, and from 135 to 138 degrees at $n_c = 19$.

Pearcy and Yang (1998); King et al. (2004)).

Let us remark incredible precision of the divergence angle. As already mentioned, it is no less astonishing than the widely noticed fact that divergence angles converge on one of the special irrational numbers. Let us take the specimen No. 13 as an example. The divergence angle of the $\frac{47}{154}$ phyllotaxis is a rational number $360\alpha \simeq 109.870^\circ$. This is very close to an irrational, ideal angle of $\alpha_0 = [3, 3]$, or $360\alpha_0 \simeq 109.877^\circ$. According to Table 20, the range of α_0 for the $\frac{47}{154}$ phyllotaxis is very narrow, that is,

$$109.831^\circ < 360\alpha_0 < 109.895^\circ, \quad (3)$$

or $360\alpha_0 \simeq 109.863 \pm 0.032$ degrees. The relative precision is less than about a part per three thousand. For reference, we present results that would be obtained if α_0 happens to be off the narrow range of (3). Instead of $\frac{47}{154}$ and the parastichy pair (59, 95) for (3), we would have obtained $\frac{43}{141}$ and (59, 82) if α_0 were slightly below the lower limit of (3), or $\alpha = \frac{40}{131}$ and (36, 95) if α_0 were above the upper limit of (3). Neither of the last two cases is listed in Tables 1~18, for they are hardly ever likely to occur. The plants’ ability to distinguish $\frac{47}{154}$ from $\frac{43}{141}$ and $\frac{40}{131}$ is due to high precision regulation of initial divergence angle. The range width of α_0 depends not so much on α_0 as on n_c . Indeed, we find $\Delta\alpha_0 \simeq (\tau/n_c)^2$ according to Eq. (B.39) in Okabe (2011). The precision as high as the above cannot be attained by a limited number of cells on the apex (Koch et al. (1998); Meinhardt et al. (1998); Smith et al.

(2006a)). It seems very unlikely that existing causal models can explain this anomalous phyllotaxis with this precision in this probability of one out of thirteen specimens.

Diversities of phyllotaxis is considered as a result of selective pressures being ineffective. In extant plants, the main Fibonacci phyllotaxis is dominant while some species specifically show very diverse phyllotaxis (Zagórska-Marek (1994)). In general, the trait diversity will be reduced if there is selective pressure acting on it. Strength of selective pressure depends specifically on extra cost required while rearranging phyllotactic patterns of leaf traces during growth of individual plants. Accordingly, the diversity may be preserved for some reason or other, e.g., when leaf traces are so fragile that the energy cost of rearrangement is insignificant. This view is consistent with recent research on *Licopodium* revealing a link between variability of leaf traces and diversity of phyllotaxis (Gola et al. (2007)). In contrast, the diversity in phyllotaxis of scale trees is considered as a result of strong selective pressure of insufficient time durations, strong because divergence angles are highly accurate whereas insufficient because various angles besides 137.5° are still in existence. In discussing diversity of phyllotaxis, one should make a clear distinction between the variance, or standard deviation, of divergence angle of an individual and varieties of divergence angles of individuals. This section was devoted to the latter, while the former was discussed in the last section.

5. Phyllotaxis and vascular organization

Girolami (1953) investigated the relation between phyllotaxis and vascular organization of *Linum* (flax), whose vascular structures of a $\frac{5}{13}$, $\frac{5}{18}$ and $\frac{8}{21}$ phyllotaxis are given in the left, center and right of Fig. 13, respectively. On the one hand, the genetic spirals of the $\frac{5}{13}$ and $\frac{5}{18}$ phyllotaxis wind up to the right (counterclockwise), while it goes to the left (clockwise) for the $\frac{8}{21}$ phyllotaxis. On the other hand, the main parastichies of the three patterns run in the same direction. That is to say, 5-parastichies for $\frac{5}{13}$ (1-6-11-16-21, etc.), 7-parastichies for $\frac{5}{18}$ (1-8-15-22-29, etc.) and 8-parastichies for $\frac{8}{21}$ (1-8-15-22-29, etc.) run steeply from the bottom right to top left (clockwise). The most direct vascular connection goes along the main parastichies. The vascular bundles of these parastichies are recognized as sectioned clusters in a transverse section of the stem, called parastichy sectors. As shown in the inset of Fig. 13, the $\frac{5}{13}$ phyllotaxis stem is divided into five parastichy sectors. In what follows, the following points remarked by Girolami (1953)

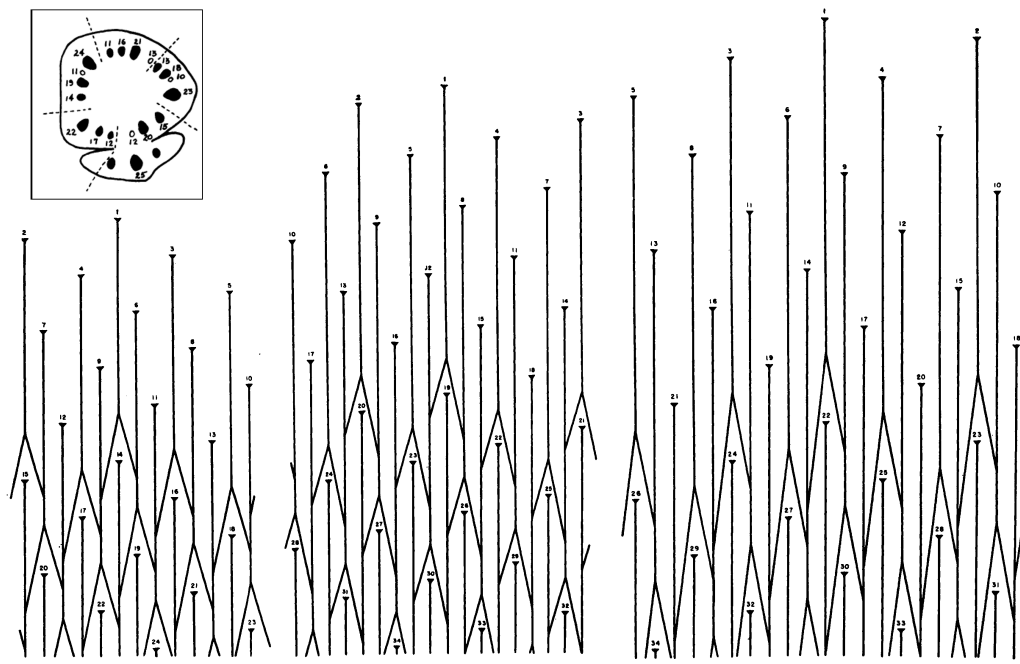


Figure 13: Diagrams of the primary vascular system of $\frac{5}{13}$ (left), $\frac{5}{18}$ (center), $\frac{8}{21}$ (right) phyllotaxis of *Linum usitatissimum*. In the inset (top left), dashed lines mark off five parasitichy sectors in a transverse section of the $\frac{5}{13}$ phyllotaxis stem. Adapted from Girolami (1953).

are analyzed in terms of the model, whereby some useful general rules are pointed out:

(G1) The number of the parastichy sectors (5, 7 and 8 for $\frac{5}{13}$, $\frac{5}{18}$ and $\frac{8}{21}$, respectively) agrees with the numerator of the phyllotactic fraction for $\frac{5}{13}$ and $\frac{8}{21}$ of the main sequence, but not for $\frac{5}{18}$ of the accessory sequence.

(G2) The length of leaf traces per internode increases with the number of parastichy sectors, namely 12 for $\frac{5}{13}$, 17 for $\frac{5}{18}$, and 19 for $\frac{8}{21}$ approximately.

(G3) There is no correlation in the relative directions of the genetic spiral and the parastichies.

As noted in the first point, there is no easy-to-use general formula between the parastichy numbers and the phyllotactic fraction (see below however), but the numerical correspondence is immediately read from Fig. 7 and Tables 1~18. According to Table 2, the parastichy pair of the $\frac{5}{18}$ phyllotaxis is (7, 11). The number of parastichy sectors is the small number of the parastichy pair. Therefore, the number 7 of the parastichy sectors of the $\frac{5}{18}$ phyllotaxis is obtained. Unlike the numerator, the denominator satisfies simple rules. Most notably, the denominator of a fraction is equal to the sum of the contact parastichy pair corresponding to the fraction (e.g. $18 = 7 + 11$). Mathematical relations between various numbers in phyllotaxis have been investigated since early times on an empirical ground based on purely mathematical properties of a regular lattice (Bravais and Bravais (1837); Naumann (1845); Jean (1994)).

On the second point, Tables 1 and 2 give the conditions $8 \leq n_c < 13$, $11 \leq n_c < 18$ and $13 \leq n_c < 21$ for the phyllotactic fractions $\frac{5}{13}$, $\frac{5}{18}$ and $\frac{8}{21}$, respectively. The predictions of the model are supported by the reported values $n_c = 12, 17$ and 19 , which satisfy their respective conditions near their upper limits. Nevertheless, a close look at Fig. 13 indicates that these figures are not accurate. As a matter of fact, n_c appears not constant but somewhat larger in the upper part of the stem. Changes in length of the leaf traces are revealed in a more sophisticated analysis of Meicenheimer (1986), where progressive transitions from $\frac{1}{3}$ through $\frac{2}{5}$ and $\frac{3}{8}$ up to $\frac{5}{13}$ have been reported. Phyllotactic transition caused by changes in n_c is discussed in the next section.

On the third point, a general rule holding between directions of parastichies and the genetic spiral is presented based on Fig. 7. To this end, it is convenient to introduce a ‘mother’ fraction of a fraction α , which is defined as the fraction lying immediately below the fraction α in the tree of Fig. 7. The mother fractions of $\frac{5}{13}$, $\frac{5}{18}$ and $\frac{8}{21}$ are $\frac{3}{8}$, $\frac{3}{11}$ and $\frac{5}{13}$, respec-

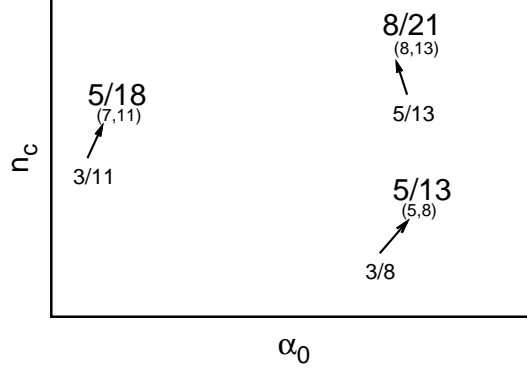


Figure 14: Three branches from Fig. 7 with which to explain spiral directions of $\frac{5}{13}$, $\frac{5}{18}$, $\frac{8}{21}$ phyllotaxis. As the fraction $\frac{5}{18}$ and $\frac{5}{13}$ are numerically bigger than their ‘mother’ fraction $\frac{3}{11}$ and $\frac{3}{8}$, their main parastichies of 7 and 5 are contrary in direction to the genetic spiral. On the contrary, 8 parastichies for $\frac{8}{21}$ are in the same direction as the genetic spiral.

tively. It is shown that *if and only if a phyllotactic fraction α is numerically bigger than its mother fraction, the main parastichies run in the direction opposite to the genetic spiral.* (The main parastichies are gentle, long spirals characterized by the small number of the contact parastichy pair.) The fraction $\alpha = \frac{5}{18}$ and $\frac{5}{13}$ are bigger than the mother fraction $\frac{3}{8}$ and $\frac{3}{11}$, respectively, while $\alpha = \frac{8}{21}$ is smaller than the mother fraction $\frac{5}{13}$. The magnitude relations are schematically shown in Fig. 5 extracted from Fig. 7. Thus, the above rule explains Girolami’s observation consistently. In practice, this rule may be used to identify the direction of the genetic spiral of a high order phyllotactic pattern for which parastichies are far easy to follow visually. Some special cases of this general rule have been remarked (Church (1904)(p. 96), Namboodiri and Beck (1968)) and occasionally taken up for discussion (Meicenheimer (1986); Fredeen et al. (2002)). The directional relations between various spirals of a phyllotactic pattern are also mathematical consequences of the regularity of the phyllotactic pattern.

The mother fraction enables us to state general rules for the phyllotactic fraction and the parastichy number: One of the parastichy pair for a fraction α is equal to the denominator of the mother fraction of α ; The other number in the pair is determined such that the sum of the pair is equal to the denominator of α . Consider $\alpha = \frac{5}{18}$, for instance. One of its parastichy

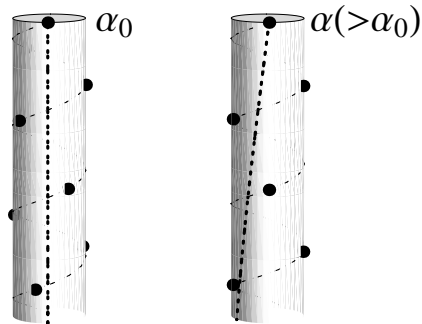


Figure 15: When the final divergence α is numerically bigger than the initial divergence α_0 , the stem is twisted in the direction of the genetic spiral. N.B. Divergence angles are less than 180 degrees.

pair is the denominator 11 of the mother fraction $\frac{3}{11}$, while the other is the difference of the denominators, $18 - 11 = 7$. As a result, the parastichy pair (7, 11) is obtained for $\frac{5}{18}$. Thus, the rules are used to relate the parastichy numbers and the phyllotactic fraction.

The vascular systems shown in Fig. 13 form closed networks. In each system, connections between leaf traces are formed along both the paired parastichies, so that the vascular bundles are divided into parastichy sectors. Among dicotyledons with helical phyllotaxis, however, an open vascular system is rather common (Beck et al. (1982)). Primitive angiosperms and many gymnosperms have open vascular systems (Beck (2010)). According to Beck et al. (1982), open systems of five sympodia (a $\frac{2}{5}$ phyllotaxis) characterize 67% of the species with helical phyllotaxy and are clearly a common type among dicotyledons. In an open system, leaf traces are connected along one direction. Although the present model determines the basic architecture of vascular phyllotaxis, it does not specify detailed structure of the reticulate pattern, whether it remains open or becomes closed. This is not a shortcoming of the model, because actual linkages between leaf traces are likely to be secondary events depending on circumstances (Kang et al. (2003)).

To conclude this section, let us remark another obvious correlation between the direction of the genetic spiral and the secondary torsion of the stem. The initial divergence α_0 is related to the fractional divergence α of a mature pattern by the angle of twist $\alpha - \alpha_0$ undergone in the secondary tor-

sion. The direction of the torsion is the same as the genetic spiral if and only if $\alpha > \alpha_0$. This is shown schematically in Fig. 5. The direction of the secondary torsion would not be difficult to check experimentally. In most typical cases, the direction is reversed, or the sign of $\alpha - \alpha_0$ changes, as n_c crosses a threshold of phyllotactic transition. Bravais and Bravais (1837) evaluated the limit divergence α_0 from mature shoots by correcting the torsion angle $\alpha - \alpha_0$.

6. Phyllotactic transition

Larson (1977) has investigated phyllotactic transition in the vascular system of *Populus* (cottonwood). His result showing transition from a $\frac{2}{5}$ to $\frac{3}{8}$ phyllotaxis is reproduced in Fig. 16. Each leaf has three traces; central, right and left traces are indicated with crosses, filled and open triangles, respectively. The leaf traces are connected with the stem vascular bundles to make sympodia. The sympodia are separated from each other, or the vascular system is open. The three traces leading to each leaf primordium arise on different sympodia. The number of the sympodia changes from five in the lower portion to eight in the upper portion of Fig. 16. The number agrees with the denominator of the phyllotactic fraction in each part. The region of the $\frac{2}{5}$ phyllotaxis occurs in the basal stem above some primary leaves, while the $\frac{3}{8}$ phyllotaxis occurs at mid and upper stem levels, principally in the zone of expanding leaves (Larson (1977)). In Fig. 16, once the transition is initiated at a point IA on a sympodium number 2, it progresses through the sympodia at points IB through IE. Three new central traces to establish the three additional sympodia of the $\frac{3}{8}$ system are derived from left traces in sequence at points IIA-IIC. Various interrelations between phyllotaxis and leaf development have been studied (Larson (1980)). In what follows, a correlation between phyllotactic transition and lengths of the leaf traces is analyzed by means of the model, whereby supporting evidence of the model is pointed out.

The lengths per internode of the leaf traces are optically read from Fig. 16 and plotted in Fig. 17. Arrows indicating the transition region between the $\frac{2}{5}$ and $\frac{3}{8}$ phyllotaxis in Fig. 17 are marked in accordance with Fig. 16 after Larson (1977). By comparison, a dashed line at $n_c = 5$ is drawn to indicate the theoretical threshold between the $\frac{2}{5}$ and $\frac{3}{8}$ phyllotaxis (Table 1). In accordance with the model, the phyllotactic transition is triggered

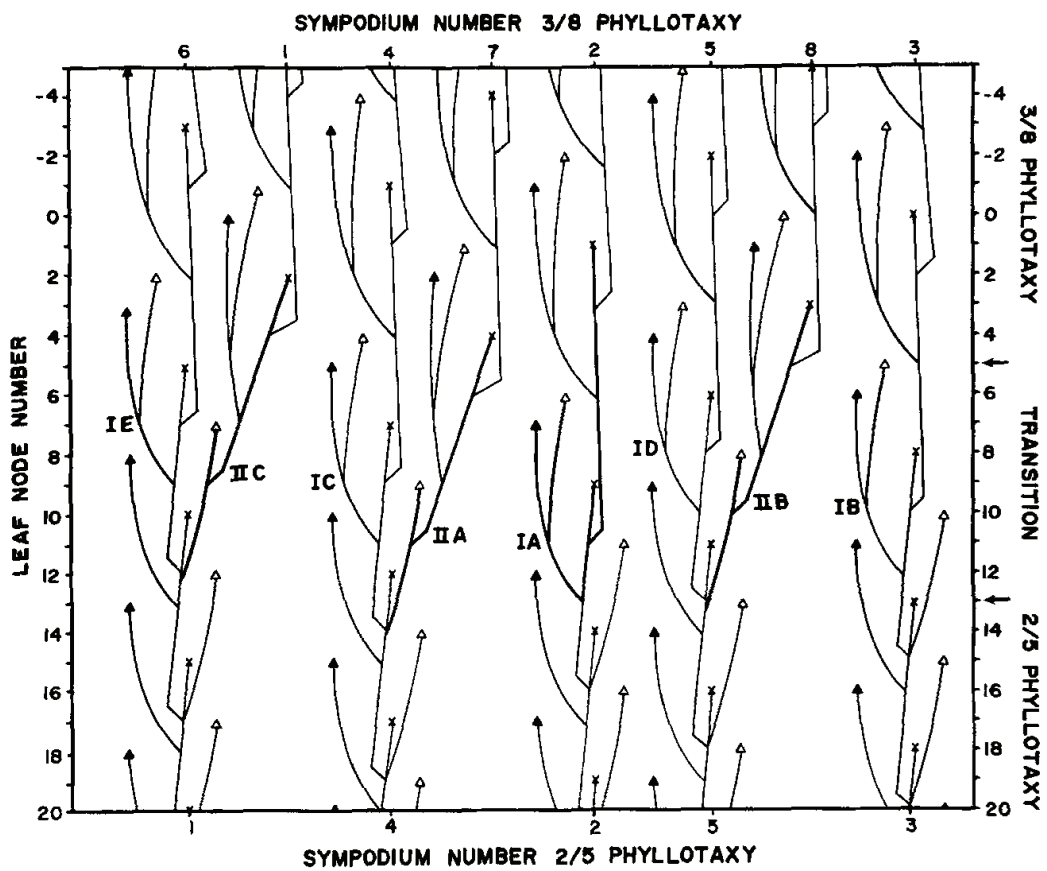


Figure 16: Transition in the primary vascular system of a cottonwood plant from a $\frac{2}{5}$ to $\frac{3}{8}$ phyllotaxis. Central, right and left traces are indicated with crosses, filled and open triangles, respectively. After Larson (1977).

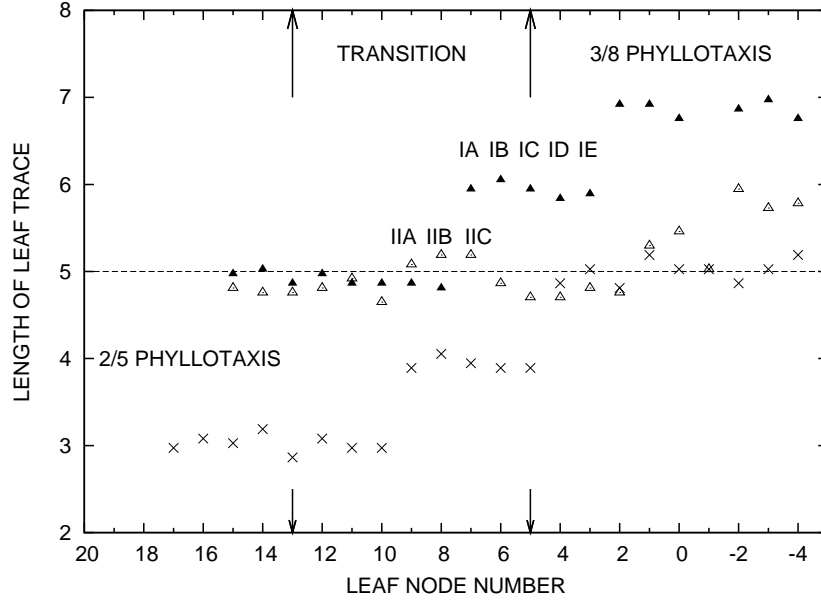


Figure 17: Length per internode of the leaf traces in Fig. 16 is plotted against the leaf node number, the vertical axis of Fig. 16. Arrows for a transition region between the $\frac{2}{5}$ and $\frac{3}{8}$ phyllotaxis and labels IA-IE and IIA-IIC to indicate initiation of the transition are marked in accordance with Fig. 16 by Larson. The phyllotactic transition is consistent with the threshold value of $n_c = 5$ predicted by the model (Table 1).

by the increasing length of the leaf traces crossing a threshold value of five internodes.

According to Table 1, phyllotactic transition is predictable. Transitions of the main sequence occur whenever the trace length n_c crosses Fibonacci numbers. The trace length, like other parameters of the plant, is predictably correlated with plant vigor (Larson (1980)). Therefore, in principle, the model allows us to control phyllotaxis artificially. In Sec. 2, leaf traces are assumed to have a common length. As noted at the end of the last section, the direction of the secondary torsion is reversed when n_c crosses a threshold value, so that it may be fixed by a leaf trace of length longer than the threshold. Fig. 18 schematically shows that long leaf traces 10, 11 and 12 trigger a transition from $\frac{2}{5}$ to $\frac{3}{8}$. In the transition region of Fig. 17, three left traces (open triangles) of the node number 7, 8 and 9 are the first to cross the threshold at $n_c = 5$. These are the very traces labeled with IIA, IIB and IIC

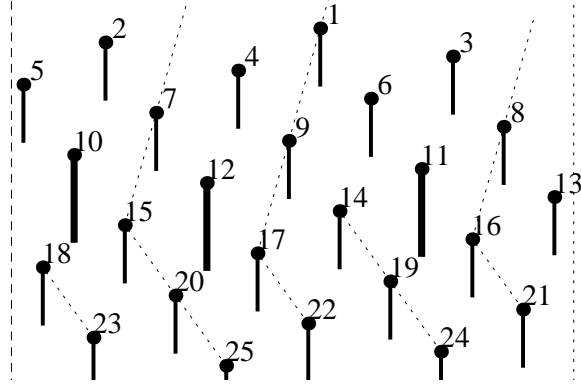


Figure 18: A phyllotactic pattern with $\alpha_0 = 1/(1 + \tau)$ (cf. Fig. 3(a)). Length of leaf traces is $n_c = 4$ (solid bars) except for 10, 11 and 12 with $n_c = 6$ (bold bars). The longer traces can induce a transition from $\alpha = \frac{2}{5}$ in the lower portion (cf. Fig. 3(b)) to $\alpha = \frac{3}{8}$ in the upper portion (cf. Fig. 5(b)). At the transition, the longer traces deflect main parastichies (dotted lines), and the parastichy number increases from 5 to 8.

by Larson as those from which the three extra sympodia branch. A close look at Fig. 16 reveals that central traces below and above the transition region are inclined in the opposite direction. This is consistent with the prediction of the model, for $\alpha = \frac{3}{8} < \alpha_0 < \frac{2}{5}$. Furthermore, five right traces (filled triangles) striking around $n_c \simeq 6$ in Fig. 17 agree with the special traces labeled with IA through IE. Thus, the observation supports the special role of the Fibonacci number 5 for the trace length n_c .

Two-step transition from a $\frac{2}{5}$ to $\frac{5}{13}$ phyllotaxis is shown in Fig. 19 after Larson (1977), where steady increase in length of leaf traces is more obvious than Fig. 16. Fig. 20 is obtained from Fig. 19 in the same manner as Fig. 17 is obtained from Fig. 16. Leaf positions at which the $\frac{3}{8}$ phyllotaxis starts and ends are marked on the right side of Fig. 19 by Larson (1977), according to which the transient pattern of the $\frac{3}{8}$ phyllotaxis is maintained for the leaves with plastochron index from 5 to -7 . Accordingly, the corresponding positions are marked by arrows in Fig. 20. On the other hand, horizontal lines at Fibonacci numbers 3, 5, and 8 in Fig. 20 theoretically divide the regions for the $\frac{1}{3}$, $\frac{2}{5}$, $\frac{3}{8}$ and $\frac{5}{13}$ phyllotaxis (Table 1). Thus, it is confirmed again that continuous changes in length of leaf traces cause discontinuous transitions in the vascular structure.

Fig. 20 indicates that n_c increases steadily up to an upper bound of about

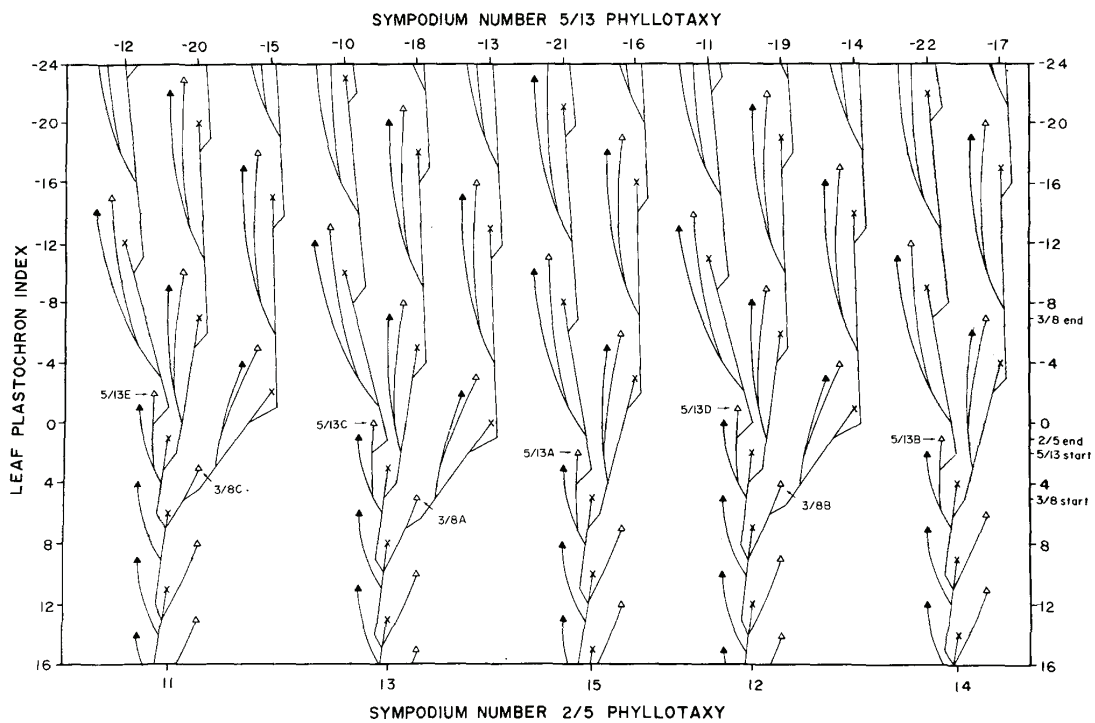


Figure 19: Reconstructed vascular system of a cottonwood plant showing transition from $\frac{2}{5}$ through $\frac{3}{8}$ to $\frac{5}{13}$ phyllotaxis by Larson (1977). See Fig. 16 for symbols.

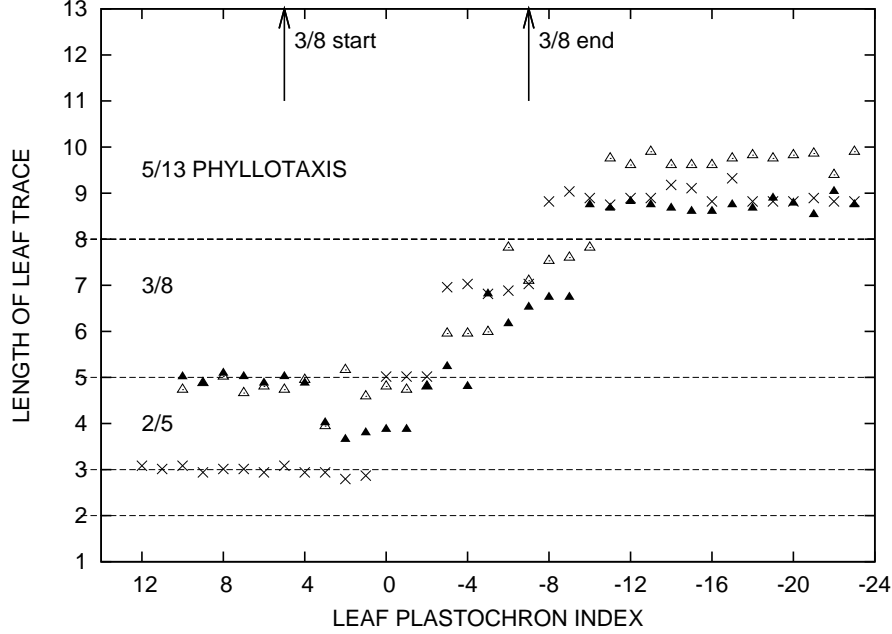


Figure 20: Length per internode of the leaf traces read from Fig. 19 is plotted against the leaf index (the vertical axis of Fig. 19). Two arrows at the top indicate where the $\frac{3}{8}$ phyllotaxis starts and ends according to Larson (1977) (see Fig. 19). According to the theoretical model, stable regions for the $\frac{2}{5}$, $\frac{3}{8}$ and $\frac{5}{13}$ phyllotaxis are separated by horizontal dashed lines at Fibonacci numbers 3, 5 and 8 (cf. Table 1). Thus, Larson's estimate of the region of the $\frac{3}{8}$ phyllotaxis agrees with the theory. Left traces (open triangles) reaching a maximum length of about 10 internodes is consistent with an observation that the highest-order phyllotactic fraction that this plant attains is $\frac{5}{13}$.

10. This observation is consistent with the fact that the $\frac{5}{13}$ phyllotaxis was the stable pattern of the old plant (Larson (1980)). According to the model, the $\frac{5}{13}$ phyllotaxis is stable insofar as n_c lies between 8 and 13, i.e., there is a 5-internode allowance for the trace length of the $\frac{5}{13}$ phyllotaxis. The main sequence is special for this wide clearance between successive threshold values. The interval is denoted as Δn_c in Okabe (2011). As shown there, the widest clearances are achieved for Fibonacci numbers, and a sequence of Fibonacci numbers is realized when the limit divergence angle is one of the special irrational numbers related to the golden ratio. As shown in Fig. 8, the number of transitions encountered while n_c grows up to above 10 is kept to a minimum number insofar as the initial divergence is restricted within

$\frac{3}{8} < \alpha_0 < \frac{3}{7}$ (from 135° to 154° , as noted at the end of Sec. 2). When n_c becomes larger than 12, the range is narrowed to $\frac{3}{8} < \alpha_0 < \frac{2}{5}$ (from 135° to 144°). Thus, the normal phyllotaxis of the main sequence is singled out. Owing to the observation that the highest-order fraction was $\alpha = \frac{5}{13}$, the model predicts that the initial divergence α_0 should be contained within $\frac{3}{8} < \alpha_0 < \frac{2}{5}$, just as observed by Fujita (1939) for other species (Sec. 2). Unfortunately, initial divergences of the cottonwood plant are not available to us. To support this argument, Puławska (1965) has reported for *Actinidia arguta* (hardy kiwi) that initial divergence remains constant despite changes in the vascular organization between $\frac{3}{8}$, $\frac{5}{13}$ and $\frac{8}{21}$.

When n_c is increased past 8, the model predicts vascular phyllotaxis of either $\alpha = \frac{5}{13}$ or $\alpha = \frac{5}{12}$ depending on whether the initial divergence α_0 is smaller or larger than $\frac{2}{5}$ (angle of 144°). Suppose $\alpha_0 = [3]$ (99.5°), then one should have five threshold lines at 2, 3, 4, 7 and 11 (Table 2), instead of four thresholds at 2, 3, 5 and 8 for $\alpha_0 = [2]$ in Fig. 20. If the initial divergence were $\alpha_0 = [5]$ (64.1° in Table 4), one should have six threshold lines at $n_c = 2, 3, 4, 5, 6$ and 11 separating patterns of $\alpha = \frac{1}{2}, \frac{1}{3}, \frac{1}{4}, \frac{1}{5}, \frac{1}{6}, \frac{2}{11}$ and $\frac{3}{17}$ (cf. Fig. 8). The vascular phyllotaxis is very unstable. The instability is energetically unfavorable. Therefore, $\alpha_0 = [5]$ (64.1°) is very improbable to survive natural selection because of the multiplicity of expected transitions. A general remark should be made when discussing multiple patterns in sequence. In order for a pattern with a definite value of α to be distinguished as such, the pattern should consist of more leaves than the denominator of the fraction α . This holds true if n_c varies sufficiently gradually; otherwise phyllotaxis transition may not be distinctly discernible.

Last but not least, whorled phyllotaxis has not been discussed in this paper. A J -jugate pattern with J fundamental spirals is formed when J leaves are borne at each node. Compared with a helical phyllotaxis with $J = 1$, divergence angles of a J -jugate system are divided by J and the parastichy pairs (m, n) are multiplied by J . Therefore, one obtains $0 < J\alpha_0 < \frac{1}{2}$ and $J(m, n)$ for the divergence angle and parastichy pair of a J -jugate system. It is known that sometimes vascular structure may change between helical and whorled phyllotaxis during ontogeny. This type of ‘anomalous’ phyllotactic transition also appears to be caused by a decrease in length of leaf traces (Jensen (1968); Beck et al. (1982); Kwiatkowska (1995)). The present model gives $\alpha = \frac{1}{2}$ for $1 \leq n_c < 2$ and $\alpha = \frac{1}{3}$ for $2 \leq n_c < 3$ irrespective of α_0 . Correspondingly, it seems natural to consider that a whorled phyllotaxis is a variation of the most primitive alternate phyllotaxis and that a whorled phyllotaxis is

triggered as n_c becomes less than 1. However, changes in the vascular structure have to be coordinated with changes in the positioning of initiated leaf primordia while a whorled pattern is established (Zagórska-Marek (1994); Meicenheimer (1998); Kelly and Cooke (2003)). The physiological processes involved are unlikely to be amenable to simple mathematical analysis. Still, a similar transition rule as a helical pattern should hold for an established whorled pattern in terms of trace length redefined with a new internode.

7. Conclusions

The present work puts forward an important role of Fibonacci numbers as critical values of the length per internode of leaf traces played in vascular phyllotaxis transition.

The regular arrangement of leaves and the regularity in divergence angle of 137.5° are a result of selective pressure to reduce possible changes in the vascular structure during growth, i.e., aperiodic arrangements will necessitate extra nutrients to reconstruct the sectorial or fractional order of vascular connections.

The phyllotactic fraction α of mature patterns of leaf traces normally makes transitions through $\frac{1}{2}, \frac{1}{3}, \frac{2}{5}, \frac{3}{8}, \frac{5}{13}, \frac{8}{21}, \dots$, whenever the number of internodes traversed by the leaf traces, n_c , crosses Fibonacci numbers, 1, 2, 3, 5, 8, 13, 21, \dots . The Fibonacci numbers make appearances because initial divergence angle α_0 of leaves at the shoot apex is normally the golden angle of about 137.5° with a good precision. The golden angle is prevalent because it is the selectively advantageous angle at which the number of the phyllotactic transition is the minimum (Fig. 8). The precision of the initial divergence is determined by the trace length n_c .

Acknowledgement

The author would like to thank Prof. Rolf Rutishauser for valuable comments on *Picea abies* and others. He would like to thank Prof. Beata Zagórska-Marek for informing him about a different view on divergence angle.

Appendix A. Relation between the trace length n_c and the plastochron ratio a

A point on a cylinder surface is located with the angular coordinate φ and the height z . Leaves on a stem are represented by a lattice of points

given by $\varphi = 2\pi\alpha n$ (in radians) and $z = hn$, where α is a constant angle of divergence, h an internode length, and n is an integer index. On the other hand, a point on a plane is located in a polar coordinate system (r, φ) , where r and φ is the radial distance from the central axis and the angular coordinate about the axis, respectively. Leaf primordia at a shoot apex are represented by $r = a^n$ and $\varphi = 2\pi\alpha n$, where a is a plastochron ratio. In a conformal growth preserving angles, the two representations are related by $2\pi z = \log r$. Hence, the internode length h corresponds to the logarithm of the plastochron ratio, $\frac{1}{2\pi} \log a$. The number of internodes traversed by the leaf traces is $n_c = Z_{lt}/h = 2\pi Z_{lt}/\log a$, where Z_{lt} is a length of leaf traces in the stem. Therefore, n_c may be regarded as inversely proportional to $\log a$, or the relative growth rate per plastochron $\frac{dr}{dn}/r$. The growth rate should depend on cell types. Accordingly, n_c may change during plant growth.

The plastochron ratio may change as a result of alteration in size of the apex and primordia. Richards (1951) discussed changing phyllotaxis to the effect that a continuous shift in the parastichy pair of normal Fibonacci phyllotaxis is linearly correlated with a double logarithm $\log(\log a)$. He defined the phyllotaxis index (P.I.) by

$$\text{P.I.} = 0.38 - 2.39 \log_{10} \log_{10} a, \quad (\text{A.1})$$

where numerical values are chosen such that the index assumes an integral value whenever two sets of parastichies in the Fibonacci system intersect orthogonally. The crossing angle between the contact parastichies changes continuously as a function of the plastochron ratio. In this descriptive model, the divergence angle α_0 is fixed at the golden angle.

Changing phyllotaxis due to change in the plastochron ratio is consistent with the present model of vascular phyllotaxis. In this model, the divergence α on the stem changes discontinuously, however. To show a correspondence between changes in phyllotaxis on the apex and the stem, let us consider the normal phyllotaxis with an initial divergence of the golden angle $\alpha_0 = \tau^{-2}$ (Table 1). Let us introduce the Fibonacci sequence F_n generated from initial integers $F_1 = 1$ and $F_2 = 1$ by the recurrence relation $F_{n+2} = F_{n+1} + F_n$. Accordingly, $F_n = 1, 1, 2, 3, 5, 8$ and 13 for $n = 1, 2, 3, 4, 5, 6$ and 7 , respectively. In terms of F_n , the phyllotactic fraction $\alpha = \frac{F_n}{F_{n+2}}$ and the parastichy pair (F_n, F_{n+1}) are obtained for $F_{n+1} \leq n_c < F_{n+2}$, or for

$$(n+1) \log \tau - \log \sqrt{5} \leq \log n_c < (n+2) \log \tau - \log \sqrt{5}$$

owing to an approximate formula $F_n \simeq \tau^n / \sqrt{5}$ valid for large n (see below (B.31) in Okabe (2011)). Therefore, $\log n_c$ is proportional to the integer index n .

To put it concretely, we get $\alpha = \frac{1}{3}$ and the parastichy pair (1,2) for $2 \leq n_c < 3$ or

$$0.7 \leq \log n_c < 1.1,$$

$\alpha = \frac{2}{5}$ and (2,3) for $3 \leq n_c < 5$ or

$$1.1 \leq \log n_c < 1.6,$$

$\alpha = \frac{3}{8}$ and (3,5) for $5 \leq n_c < 8$ or

$$1.6 \leq \log n_c < 2.1,$$

$\alpha = \frac{5}{13}$ and (5,8) for $8 \leq n_c < 13$ or

$$2.1 \leq \log n_c < 2.6,$$

and so on. Thus, the shift in the parastichy pair is linearly correlated with $\log n_c \propto \log(\log a)$. This is a general property holding also for other initial divergences found in nature.

For the systematic study of the mature stem, the index n_c is more usefully regarded as a developmental index than a , not only because an internode is a natural unit of length as the plastochron is the developmental unit of time, but values of n_c allowed for a phyllotactic pattern are delimited by the special integers traditionally familiar to those who are enchanted by phyllotaxis; Fibonacci numbers. For a given initial divergence, the numbers comprise a sequence generated by the Fibonacci recurrence relation $F_{n+2} = F_{n+1} + F_n$ from a pair of different seed integers. The main sequence, 1, 2, 3, 5, 8, \dots in Table 1, is generated from the simplest seed pair (1,2). The next simplest seed integers (1,3) give the accessory sequence 1, 3, 4, 7, 11, 18 \dots of Table 2. In this manner, any phyllotactic sequence is characterized by a pair of seed integers, as well as the limit divergence α_0 . This is in accordance with accumulated empirical wisdom of phyllotaxis. Traditionally, these special integers have been remarked in connection with parastichy numbers (cf. Tables 1~18). The present work puts emphasis on these numbers as critical values for the length per internode of leaf traces. This point has never been remarked before.

References

- Adler, I., 1974. A model of contact pressure in phyllotaxis. *Journal of Theoretical Biology* 45, 1–79.
- Airy, H., 1873. On leaf-arrangement. *Proc. Royal Soc. London* 21, 176–179.
- Allard, H., 1942. Some aspects of the phyllotaxy of tobacco. *Journal Agricultural Research* 64, 49–55.
- Atela, G., Golé, J. A., Hotton, J. P., 2002. A Dynamical System for Plant Pattern Formation: A Rigorous Analysis. *Journal of NonLinear Science* 12, 641–676.
- Barabé, D., Bourque, L., Yin, X., Lacroix, C., 2010. Phyllotaxis of the palm *Euterpe oleracea* Mart. at the level of the shoot apical meristem. *Botany* 88 (5), 528–536.
- Beck, C. B., 2010. *An Introduction to Plant Structure and Development*. Cambridge University Press.
- Beck, C. B., Schmid, R., Rothwell, G. W., 1982. Stelar morphology and the primary vascular system of seed plants. *Botanical Review* 48, 691–815.
- Braun, A., 1831. Vergleichende Untersuchung über die Ordnung der Schuppen an den Tannenzapfen als Einleitung zur Untersuchung der Blattstellung. *Verhandlungen der Kaiserlichen Leopoldinisch-Carolinischen Akademie der Naturforscher* 15, 195–402.
- Braun, A., 1835. Dr. Carl Schimper's Vorträge über die Möglichkeit eines wissenschaftlichen Verständnisses der Blattstellung, nebst Andeutung der hauptsächlichen Blattstellungsgesetze und insbesondere der neuentdeckten Gesetze der Aneinanderreihung von Cyclen verschiedene maasse. *Flora* 18, 145–191.
- Bravais, L., Bravais, R., 1837. Essai sur la disposition des feuilles curvisériées. *Annales des Sciences Naturelles Botanique* 7, 42–110.
- Bryntsev, V. A., 2004. Types of phyllotaxis and patterns of their realization. *Russ. J. Dev. Biol.* 2, 114–156.

- Chapman, J. M., Perry, R., 1987. A diffusion model of phyllotaxis. *Annals of Botany* 60 (4), 377–389.
- Church, A. H., 1904. On the Relation of Phyllotaxis to Mechanical Laws. On the Relation of Phyllotaxis to Mechanical Laws. Williams & Norgate, London.
- Church, A. H., 1920. On the interpretation of phenomena of phyllotaxis. Botanical memoirs. Hafner Pub. Co.
- Coxeter, H. S. M., 1972. The role of intermediate convergents in Tait's explanation for phyllotaxis. *Journal of Algebra* 20, 167–175.
- Cummings, F., Strickland, J., 1998. A model of phyllotaxis. *Journal of Theoretical Biology* 192 (4), 531–544.
- Davies, P. A., 1939. Leaf position in *Ailanthus altissima* in relation to the Fibonacci series. *American Journal of Botany* 26, 67–74.
- de Candolle, C., 1881. *Considérations sur l'étude de la phyllotaxie*. Geneva: H. Georg.
- Delpino, F., 1883. Teoria generale della fillotassi. *Atti della R. Università di Genova*. Armanino.
- Dickson, A., 1871. On the phyllotaxis of *Lepidodendron* and the allied, if not identical, genus *Knorria*. *Journal of botany, British and foreign* 9, 166–167.
- Dormer, K., 1972. Shoot organization in vascular plants. *Shoot Organization in Vascular Plants*. Syracuse University Press.
- Douady, S., Couder, Y., 1996. Phyllotaxis as a dynamical self organizing process part I: The spiral modes resulting from time-periodic iterations. *Journal of Theoretical Biology* 178, 255–274.
- Erickson, R. O., 1983. The geometry of phyllotaxis. In: Dale, J., Milthorpe, F. (Eds.), *The Growth and functioning of leaves: proceedings of a symposium held prior to the thirteenth International Botanical Congress at the University of Sydney, 18-20 August 1981*. Cambridge University Press, pp. 53–88.

- Erickson, R. O., Michelini, F. J., 1957. The plastochron index. *American Journal of Botany* 44, 297–305.
- Esau, K., 1965. *Vascular differentiation in plants*. New York: Holt, Rinehart and Winston.
- Fredeen, A. L., Horning, J. A., Madill, R. W., 2002. Spiral phyllotaxis of needle fascicles on branches and scales on cones in *pinus contorta* var. *latifolia*: Are they influenced by wood-grain spiral? *Canadian Journal of Botany* 80 (2), 166–175.
- Fujita, T., 1937. Über die Reihe 2,5,7,12.... in der schraubigen Blattstellung und die mathematische Betrachtung verschiedener Zahlenreihensysteme. *Bot. Mag. Tokyo* 51, 298–307.
- Fujita, T., 1938. Statistische Untersuchung über die Zahl der konjugierten Parastichen bei den schraubigen Organstellungen. *Bot. Mag. Tokyo* 52, 425–433.
- Fujita, T., 1939. Statistische Untersuchungen über den Divergenzwinkel bei den schraubigen Organstellungen. *Bot. Mag. Tokyo* 53, 194–199.
- Girolami, G., 1953. Relation between phyllotaxis and primary vascular organization in *linum*. *American Journal of Botany* 40, 618–625.
- Gola, E. M., Jernstedt, J. A., Zagórska-Marek, B., 2007. Vascular architecture in shoots of early divergent vascular plants, *Lycopodium clavatum* and *Lycopodium annotinum*. *New Phytologist* 174 (4), 774–786.
- Green, P. B., Steele, C. S., Rennich, S. C., 1996. Phyllotactic Patterns: A Biophysical Mechanism for their Origin. *Annals of Botany* 77, 515–527.
- Hellwig, H., Engelmann, R., Deussen, O., 2006. Contact pressure models for spiral phyllotaxis and their computer simulation. *Journal of Theoretical Biology* 240 (3), 489–500.
- Hirmer, M., 1922. *Zur Lösung des Problems der Blattstellungen*. G. Fischer.
- Hirmer, M., 1931. *Zur Kenntnis der Schraubenstellungen im Pflanzenreich*. *Planta* 14, 132–206.

- Hofmeister, W., 1868. Allgemeine Morphologie der Gewächse. In: de Bary, A., Irmisch, T. H., Sachs, J. (Eds.), *Handbuch der Physiologischen Botanik*. Leipzig: W. Engelmann, pp. 405–664.
- Hotton, S., Johnson, V., Wilbarger, J., Zwieniecki, K., Atela, P., Golé, C., Dumais, J., 2006. The possible and the actual in phyllotaxis: Bridging the gap between empirical observations and iterative models. *Journal of Plant Growth Regulation* 25, 313–323.
- Jean, R., 1986. An interpretation of Fujita's frequency diagrams in phyllotaxis. *Bulletin of Mathematical Biology* 48, 77–86.
- Jean, R. V., 1994. *Phyllotaxis: A Systemic Study in Plant Morphogenesis*. Cambridge Univ. Press, Cambridge, New York.
- Jensen, L. C. W., 1968. Primary stem vascular patterns in three subfamilies of the Crassulaceae. *American Journal of Botany* 55, 553–563.
- Jönsson, H., Heisler, M. G., Shapiro, B. E., Meyerowitz, E. M., Mjolsness, E., 2006. An auxin-driven polarized transport model for phyllotaxis. *Proceedings of the National Academy of Sciences of the United States of America* 103 (5), 1633–1638.
- Kang, J., Tang, J., Donnelly, P., Dengler, N., 2003. Primary vascular pattern and expression of *ATHB-8* in shoots of *arabidopsis*. *New Phytologist* 158 (3), 443–454.
- Kelly, W. J., Cooke, T. J., 2003. Geometrical relationships specifying the phyllotactic pattern of aquatic plants. *American Journal of Botany* 90 (8), 1131–1143.
- King, S., Beck, F., Lüttge, U., 2004. On the mystery of the golden angle in phyllotaxis. *Plant, Cell & Environment* 27 (6), 685–695.
- Kirchoff, B. K., 1984. On the relationship between phyllotaxy and vasculature: a synthesis. *Botanical Journal of the Linnean Society* 89, 37–51.
- Kirchoff, B. K., 2003. Shape Matters: Hofmeister's Rule, Primordium Shape, and Flower Orientation. *International Journal of Plant Sciences* 164 (4), 505–517.

- Koch, A.-J., Bernasconi, G., Rothen, F., 1998. Phyllotaxis as a geometrical and dynamical system. In: Jean, R. V., Barabé, D. (Eds.), Symmetry in plants. World Scientific, pp. 459–486.
- Koch, A. J., Meinhardt, H., 1994. Biological pattern formation: from basic mechanisms to complex structures. Review of Modern Physics 66, 1481–1507.
- Kuhlemeier, C., 2007. Phyllotaxis. TRENDS in Plant Science 12, 143–150.
- Kumazawa, M., Kumazawa, M., 1971. Periodic variations of the divergence angle, internode length and leaf shape, revealed by correlogram analysis. Phytomorphology 21, 376–389.
- Kunz, M., September 2001. Dynamical models of phyllotaxis. Phys. D 157, 147–165.
- Kwiatkowska, D., 1995. Ontogenetic changes in the shoot primary vasculature of *Anagallis arvensis* L. Acta Societatis Botanicorum Poloniae 64, 213–222.
- Larson, P. R., 1977. Phyllotactic transitions in the vascular system of *Populus deltoides* Bartr. as determined by ^{14}C labeling. Planta 134, 241–249.
- Larson, P. R., 1980. Interrelations between phyllotaxis, leaf development and the primary-secondary vascular transition in *Populus deltoides*. Annals of Botany 46, 757–769.
- Larson, P. R., 1983. Primary vascularization and the siting of primordia. In: Dale, J. E., Milthorpe, F. L. (Eds.), The growth and functioning of leaves. Cambridge, UK: Cambridge University Press, pp. 25–51.
- Leigh, E. G., 1972. The golden section and spiral leaf-arrangement. Transactions of the Connecticut Academy of Arts and Sciences 44, 163–176.
- Lestiboudois, M. T., 1848. Phyllotaxie anatomique. Annales des Sciences Naturelles 3, 15–105, 136–189.
- Levitov, L. S., 1991. Energetic approach to phyllotaxis. Europhys. Lett. 14, 533–539.

- Lyndon, R., 1990. Plant development: the cellular basis. Topics in plant physiology. Unwin Hyman.
- Maksymowych, R., Erickson, R. O., 1977. Phyllotactic change induced by gibberellic acid in *Xanthium* shoot apices. American Journal of Botany 64, 33–44.
- Malygin, A. G., 2006. Morphodynamics of phyllotaxis. Int. J. Dev. Biol. 50, 277–287.
- Marc, J., Hackett, W. P., 1991. Gibberellin-induced reorganization of spatial relationships of emerging leaf primordia at the shoot apical meristem in *Hedera helix* L. Planta 185, 171–178.
- Marzec, C., Kappraff, J., 1983. Properties of maximal spacing on a circle related to phyllotaxis and to the golden mean. Journal of Theoretical Biology 103, 201–226.
- Meicenheimer, R. D., 1986. Role of parenchyma in *Linum usitatissimum* leaf trace patterns. American Journal of Botany 73, 1649–1664.
- Meicenheimer, R. D., 1998. Decussate to spiral transitions in phyllotaxis. In: Jean, R. V., Barabé, D. (Eds.), Symmetry in plants. World Scientific, pp. 125–144.
- Meicenheimer, R. D., 2006. Stem unit growth analysis of *Linum usitatissimum* (Linaceae) internode development. American Journal of Botany 93 (1), 55–63.
- Meinhardt, H., Koch, A.-J., Bernasconi, G., 1998. Models of pattern formation applied to plant development. In: Jean, R. V., Barabé, D. (Eds.), Symmetry in plants. World Scientific, pp. 723–758.
- Mitchison, G. H., 1977. Phyllotaxis and the Fibonacci series. Science 196, 270–275.
- Nägeli, C. W., 1858. Das Wachstum des Stammes und der Wurzel bei den Gefäßpflanzen und die anordnung der Gefäßstränge im Stengel. Beitrage Zur Wissenschaftlichen Botanik 1, 1–156.

- Namboodiri, K. K., Beck, C. B., 1968. A comparative study of the primary vascular system of conifers. I. genera with helical phyllotaxis. *American Journal of Botany* 55, 447–457.
- Naumann, C., 1845. Ueber den Quincunx als Grundgesetz der Blattstellung vieler Pflanzen. Arnold.
- Nelson, T., Dengler, N., 1997. Leaf vascular pattern formation. *The Plant Cell Online* 9 (7), 1121–1135.
- Newell, A. C., Shipman, P. D., Sun, Z., 2008. Phyllotaxis: cooperation and competition between mechanical and biochemical processes. *Journal of Theoretical Biology* 251 (3), 421–439.
- Niklas, K. J., 1988. The role of phyllotatic pattern as a "developmental constraint" on the interception of light by leaf surfaces. *Evolution* 42, 1–16.
- Niklas, K. J., 1997. *The evolutionary biology of plants*. University of Chicago Press.
- Niklas, K. J., 1998. Light harvesting "fitness landscapes" for vertical shoots with different phyllotactic patterns. In: Jean, R. V., Barabé, D. (Eds.), *Symmetry in plants*. World Scientific, pp. 759–773.
- Okabe, T., 2011. Physical phenomenology of phyllotaxis. *Journal of Theoretical Biology* 280, 63–75.
- Pearcy, R. W., Yang, W., 1998. The functional morphology of light capture and carbon gain in the redwood forest understorey plant *Adenocaulon bicolor* hook. *Functional Ecology* 12 (4), 543–552.
- Priestley, J. H., Scott, L. I., 1933. Phyllotaxis in the dicotyledon from the standpoint of developmental anatomy. *Biological Reviews* 8 (3), 241–268.
- Priestley, J. H., Scott, L. I., 1936. The vascular anatomy of *Helianthus annuus* L. *Proc. Leeds Phil. Soc.* 3, 159–173.
- Prusinkiewicz, P., Lindenmayer, A., 1991. *The Algorithmic Beauty of Plants (The Virtual Laboratory)*. Springer.

- Puławska, Z., 1965. Correlations in the development of the leaves and leaf traces in the shoot of *Actinidia arguta* Planch. Acta Societatis Botanicorum Poloniae 34, 697–712.
- Reinhardt, D., 2005. Regulation of phyllotaxis. Int. J. Dev. Biol. 49, 539–546.
- Richards, F. J., 1948. The geometry of phyllotaxis and its origin. Symp. Soc. Exp. Biol 2, 217–245.
- Richards, F. J., 1951. Phyllotaxis: Its quantitative expression and relation to growth in the apex. Philos. Trans. R. Soc. B 225, 509–564.
- Ridley, J. N., 1982. Packing efficiency in sunflower heads. Math. Biosci. 58, 129–139.
- Rivier, N., Occelli, R., Pantaloni, J., Lissowski, A., 1984. Structure of Bénard convection cells, phyllotaxis and crystallography in cylindrical symmetry. J. Phys. (Paris) 45, 49–63.
- Roberts, D. W., 1984. A chemical contact pressure model for phyllotaxis. Journal of Theoretical Biology 108, 481–490.
- Roberts, D. W., 1987. The chemical contact pressure model for phyllotaxis – application to phyllotaxis changes in seedlings and to anomalous phyllotaxis systems. Journal of Theoretical Biology 125, 141–161.
- Rothen, F., Koch, A. J., 1989. Phyllotaxis or the properties of spiral lattices. II. packing of circles along logarithmic spirals. J. Phys. (Paris) 50, 1603–1621.
- Rutishauser, R., 1998. Plastochrone ratio and leaf arc as parameters of a quantitative phyllotaxis analysis in vascular plants. In: Jean, R. V., Barabé, D. (Eds.), Symmetry in plants. World Scientific, pp. 171–212.
- Schimper, K. F., 1835. Beschreibung des Symphytum Zeyheri und seiner zwei deutschen verwandten der *S. bulbosum* Schimper und *S. tuberosum* Jacq. Winter.
- Schoute, J. C., 1913. Beiträge zur Blattstellungslehre. Rec. Trav. Bot. Néerl 10, 153–324.

- Schwabe, W., Clewer, A., 1984. Phyllotaxis – a simple computer model based on the theory of a polarly-translocated inhibitor. *Journal of Theoretical Biology* 109, 595–619.
- Schwendener, S., 1878. *Mechanische Theorie der Blattstellungen*. Leipzig: Engelmann.
- Schwendener, S., 1883. Zur Theorie der Blattstellungen. *Sitzungsber. d. Berl. Akad. d. Wissensch* XXXII, 741–773.
- Shipman, P., Sun, Z., Pennybacker, M., Newell, A., 2011. How universal are Fibonacci patterns? *The European Physical Journal D - Atomic, Molecular, Optical and Plasma Physics* 62, 5–17.
- Skutch, A. F., 1927. Anatomy of leaf of banana, *Musa sapientum* L. var. Hort. Gros Michel. *Botanical Gazette* 84, 337–391.
- Smith, R. S., Guyomarc'h, S., Mandel, T., Reinhardt, D., Kuhlemeier, C., Prusinkiewicz, P., 2006a. A plausible model of phyllotaxis. *Proceedings of the National Academy of Sciences of the United States of America* 103 (5), 1301–1306.
- Smith, R. S., Kuhlemeier, C., Prusinkiewicz, P., 2006b. Inhibition fields for phyllotactic pattern formation: a simulation study. *Canadian Journal of Botany* 84 (11), 1635–1649.
- Snow, M., Snow, R., 1934. The interpretation of phyllotaxis. *Biological Reviews* 9, 132–137.
- Snow, M., Snow, R., 1962. A theory of the regulation of phyllotaxis based on *Lupinus albus*. *Philos. Trans. Roy. Soc. London B* 244, 483–513.
- Snow, R., 1955. Problems of phyllotaxis and leaf determination. *Endeavour* 14, 190–199.
- Steeves, T., Sussex, I., 1989. *Patterns in plant development*. Cambridge University Press.
- Sterling, C., 1945. Growth and vascular development in the shoot apex of *Sequoia sempervirens* (Lamb.) Endl. II. vascular development in relation to phyllotaxis. *American Journal of Botany* 32, 380–386.

- Takenaka, A., 1994. Effects of leaf blade narrowness and petiole length on the light capture efficiency of a shoot. *Ecological Research* 9, 109–114.
- Teitz, P., 1888. Ueber definitive Fixirung der Blattstellung durch die Torsionswirkung der Leitstränge. *Flora* 71. Jahrgang, 419–439.
- Thomas, R. L., 1975. Orthostichy, parastichy and plastochrone ratio in a central theory of phyllotaxis. *Annals of Botany* 39 (3), 455–489.
- Thompson, D. W., 1917. *On Growth and Form*. Oxford. Clarendon Press.
- Thornley, J. H. M., 1975. Phyllotaxis. I. A Mechanistic Model. *Annals of Botany* 39, 491–507.
- Unruh, M., 1950. Neue Beobachtungen über die Rhythmik der Symmetrie am zerstreut beblätterten Spross. *Berichte der Deutschen Botanischen Gesellschaft* 63, 88–96.
- Valladares, F., Brites, D., 2004. Leaf phyllotaxis: Does it really affect light capture? *Plant Ecology* 174, 11–17.
- van Iterson, G., 1907. *Mathematische und Mikroskopisch-Anatomische Studien über Blattstellungen*. G. Fischer, Jena.
- Veen, A. H., Lindenmayer, A., 1977. Diffusion mechanism for phyllotaxy. *Plant Physiol.* 60, 127–139.
- Vogel, H., 1979. A better way to construct the sunflower head. *Mathematical Biosciences* 44 (3-4), 179–189.
- Watson, M. A., Casper, B. B., 1984. Morphogenetic constraints on patterns of carbon distribution in plants. *Annual Review of Ecology and Systematics* 15, 233–258.
- Wiesner, J., 1875. Bemerkungen über rationale und irrationale Divergenzen. *Flora* 58, 113–115, 139–143.
- Wiesner, J., 1907. *Der Lichtgenuss der Pflanzen: photometrische und physiologische Untersuchungen mit besonderer Rücksichtnahme auf Lebensweise, geographische Verbreitung und Kultur der Pflanzen*. W. Engelmann.

- Williams, R., 1974. The shoot apex and leaf growth: a study in quantitative biology. Cambridge University Press.
- Williams, R. F., Brittain, E. G., 1984. A geometrical model of phyllotaxis. Australian Journal of Botany 32, 43–72.
- Wright, C., 1873. The uses and origin of the arrangements of leaves in plants. Memoirs of the American Academy of Arts and Sciences 9 (2), 379–415.
- Yotsumoto, A., 1993. A diffusion model for phyllotaxis. Journal of Theoretical Biology 162, 131–151.
- Young, D. A., 1978. On the diffusion theory of phyllotaxis. Journal of Theoretical Biology 71 (3), 421–432.
- Zagórska-Marek, B., 1985. Phyllotactic patterns and transitions in *Abies balsamea*. Canadian Journal of Botany 63 (10), 1844–1854.
- Zagórska-Marek, B., 1994. Phyllotaxic diversity in *Magnolia* flowers. Acta Societatis Botanicorum Poloniae 63, 117–137.
- Zagórska-Marek, B., Szpak, M., 2008. Virtual phyllotaxis and real plant model cases. Functional Plant Biology 35, 1025–1033.